

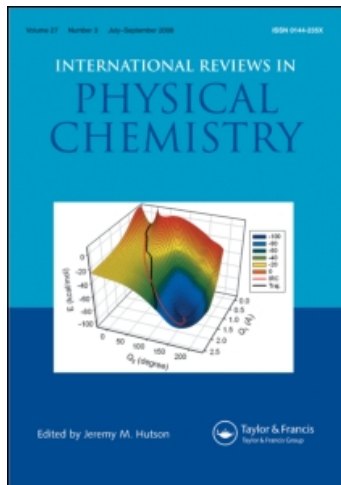
This article was downloaded by:

On: 21 January 2011

Access details: *Access Details: Free Access*

Publisher *Taylor & Francis*

Informa Ltd Registered in England and Wales Registered Number: 1072954 Registered office: Mortimer House, 37-41 Mortimer Street, London W1T 3JH, UK



## International Reviews in Physical Chemistry

Publication details, including instructions for authors and subscription information:

<http://www.informaworld.com/smpp/title~content=t713724383>

### Electron impact ionization of $C_{60}$ and $C_{70}$ : production and properties of parent and fragment ions studied with a two-sector field mass spectrometer

P. Scheier<sup>a</sup>; B. Dünser<sup>a</sup>; R. Wörgötter<sup>a</sup>; S. Matt<sup>a</sup>; D. Muigg<sup>a</sup>; G. Senn<sup>a</sup>; T. D. Måk<sup>a</sup>

<sup>a</sup> Institut für Ionenphysik, Leopold Franzens Universität, Innsbruck, Austria

**To cite this Article** Scheier, P. , Dünser, B. , Wörgötter, R. , Matt, S. , Muigg, D. , Senn, G. and Måk, T. D.(1996) 'Electron impact ionization of  $C_{60}$  and  $C_{70}$ : production and properties of parent and fragment ions studied with a two-sector field mass spectrometer', *International Reviews in Physical Chemistry*, 15: 1, 93 – 131

**To link to this Article:** DOI: 10.1080/01442359609353177

**URL:** <http://dx.doi.org/10.1080/01442359609353177>

PLEASE SCROLL DOWN FOR ARTICLE

Full terms and conditions of use: <http://www.informaworld.com/terms-and-conditions-of-access.pdf>

This article may be used for research, teaching and private study purposes. Any substantial or systematic reproduction, re-distribution, re-selling, loan or sub-licensing, systematic supply or distribution in any form to anyone is expressly forbidden.

The publisher does not give any warranty express or implied or make any representation that the contents will be complete or accurate or up to date. The accuracy of any instructions, formulae and drug doses should be independently verified with primary sources. The publisher shall not be liable for any loss, actions, claims, proceedings, demand or costs or damages whatsoever or howsoever caused arising directly or indirectly in connection with or arising out of the use of this material.

## Electron impact ionization of $C_{60}$ and $C_{70}$ : production and properties of parent and fragment ions studied with a two-sector field mass spectrometer

by P. SCHEIER, B. DÜNSER, R. WÖRGÖTTER, S. MATT, D. MUIGG,  
G. SENN and T. D. MÄRK

Institut für Ionenphysik, Leopold Franzens Universität, Technikerstr. 25, A-6020,  
Innsbruck, Austria

Electron impact ionization and dissociation studies of  $C_{60}$  and  $C_{70}$  carried out in our laboratory over the past three years have revealed many exciting and novel features of this new class of molecules (clusters). The most salient results are summarized in this paper, including first a description of the crossed beams apparatus and the various mass spectrometric (two-sector field) techniques used. This is followed by a discussion of the production of parent and fragment ions (with up to eight charges) via electron impact ionization of  $C_{60}$  and  $C_{70}$  including results on mass spectral fragmentation patterns and measured and calculated absolute ionization cross-section functions. The experimental results concerning the energetics of produced parent and fragment ions are presented in the next section and measured appearance energies and breakdown curves are analysed in the frame of various theoretical concepts (RRKM, FHBT) thereby allowing us to derive the corresponding binding energies. The last section is devoted to (i) the different aspects of the stability of singly- and multiply-charged fullerene ions (i.e. the quantitative study of various unimolecular decay channels such as monomer evaporation, sequential decay series, charge separation reactions, etc.) and, based on the measured properties of these decay reactions, to (ii) a discussion of the possible decay mechanisms.

### 1. Introduction

Since the first report about the unique structure of  $C_{60}$  by Kroto *et al.* [1] in 1985 and the discovery by Krätschmer *et al.* [2] in 1990 as to how to produce gram quantities of  $C_{60}$  (and other fullerenes), a new world of chemistry, physics and material science has developed and is growing at a tremendous rate [3]. It is important to remember that the key original experiment which allowed the bold conclusion about the special nature of  $C_{60}$  (i.e. the truncated icosahedral structure) included a positive and negative carbon cluster ion mass spectrum. During the past two years we have carried out a series of mass spectrometric investigations concerning the electron impact ionization and the electron attachment of  $C_{60}$  and  $C_{70}$ . Not too surprisingly,  $C_{60}$  (and  $C_{70}$ ) also exhibits in this respect, i.e. electron ionization and attachment, rather tantalizing properties—unparalleled by other molecular systems.

For example, the first measurements—carried out using a crossed beams apparatus—of electron attachment cross-section functions for  $C_{60}$  and  $C_{70}$  revealed an unusually large cross-section for the production of  $C_{60}^-$  and  $C_{70}^-$ , respectively [4]. It was observed, moreover, that only parent ions (and absolutely no fragment anions, which is in contrast to the situation encountered for ordinary molecules [5]) are produced by the attaching electrons and that the cross-section remained high (in the order of  $10^{-18}$  m<sup>2</sup>) from near zero electron energy up to about 10 eV and then reduced quickly to reach zero at about 15 eV electron energy. Resonance structures observed have been

attributed to electronic and vibrational excitations during the attachment (i.e. Feshbach and shape resonances, see also [6]). Subsequent to these initial studies [4], further studies [7], in which we have determined the rate coefficients for electron attachment to  $C_{60}$  using a flowing afterglow Langmuir probe apparatus, have revealed the existence of a barrier to low energy electron attachment to  $C_{60}$ . This is in accordance with recent theoretical calculations [8] showing that s-wave electron capture to  $C_{60}$  cannot occur and the apparent activation energy required for the attachment reaction has to be attributed to a centrifugal barrier to electron capture in the p-wave channel. Quantum mechanical calculations of the absolute cross-sections and corresponding rate coefficients are in good agreement with both experimental data sets (the crossed beams and the swarm technique data) and allowed us to derive the height of the activation barrier of  $C_{60}$  to be 0.26 eV.

In response to these first two studies, a more precise electron/ $C_{60}$  beam study was performed [9] concerning attachment and detachment as a function of electron energy. By deconvoluting these beam data we were able to verify the low energy barrier to  $C_{60}$  and to show that a barrier also exists to electron capture to  $C_{70}$ . The detachment rate from  $C_{60}^-$  anions increased with increasing incident electron energy (i.e. temperature of the negative ion formed), which is reminiscent of (i) thermionic emission from metal surfaces (cf. thermionic emission studies from hot  $C_{60}^-$  ions heated by directing them at high energies onto solid surfaces [10]) and (ii) another study where electron emission follows the absorption of several photons from a laser pulse [11]. Detailed analysis of these detachment data and some quantum mechanical calculations of the capture cross-sections in an additional paper [12] provided further insights into the electron attachment and detachment of  $C_{60}$ . Comparison between experimental data for the absolute attachment cross-sections and quantum calculations confirmed that attachment occurs at low energies in the p-wave channel, whereas at higher electron energies attachment also proceeds via the d-, f- and higher-order partial wave channels. At electron energies above approximately 7 eV, thermal detachment is seen to become dominant, and the unimolecular rate coefficient has been determined as a function of the energy of the attaching electron. By relating the detachment coefficient to the temperature of the hot  $C_{60}^-$ , the electron detachment energy has been obtained as 2.6 eV, which is close to the electron affinity of  $C_{60}$  as measured by photodetachment from cold  $C_{60}^-$  ions [11, 13, 14]. An important conclusion to be drawn from all these studies is that  $C_{60}$  and  $C_{70}$  (see also [15]) very efficiently capture electrons over the wide energy range from thermal up to approximately 15 eV. Furthermore, recent studies of doubly-charged anions of small carbon clusters [16] and the closed fullerenes  $C_{60}$  and  $C_{70}$  [17] firmly establish the existence of long-lived gas phase dianions in the size region where interelectron repulsion becomes large.

Also in the case of electron impact ionization a first glance at the positive mass spectrum reveals the extraordinary nature of the closed cage fullerenes, i.e. in contrast to other molecules [5, 18] in this mass range the parent ion appears to be by far the most abundant ion in the mass spectrum (see figure 1 showing a section of the  $C_{60}$  mass spectrum around the parent ion peak). As it transpired in a number of recent studies [19–42] carried out in our laboratory on the electron impact ionization of  $C_{60}$  and  $C_{70}$  there are many more exciting and novel features. The most salient results are summarized in this paper (previous results concerning electron impact ionization of the fullerenes and characterization of fullerenes by mass spectrometry, up to 1993, are reviewed in [43, 44]), including in §2 a description of the experimental set-up and the various techniques used. Section 3 covers the production of parent and fragment ions

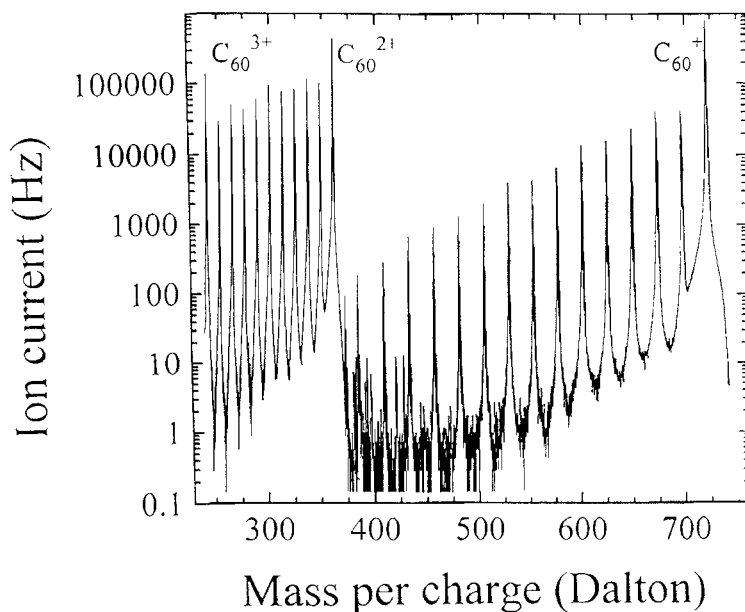


Figure 1. Section of mass spectrum (semilog scale) of  $C_{60}$  using 200 eV electrons (electron current 200  $\mu\text{A}$ ).

(with up to seven charges) via electron impact ionization of  $C_{60}$  and  $C_{70}$  including a detailed discussion of the mass spectral fragmentation pattern and measured absolute partial and total ionization cross-sections. The experimental results concerning the energetics of the produced parent and fragment ions is presented in §4 and measured appearance energies and breakdown curves are analysed in the frame of various theoretical concepts (Rice–Ramsperger–Kassel–Marcus (RRKM) and finite heat bath theory (FHBT)) thereby allowing the derivation of corresponding binding energies. Section 5 is devoted to (i) the different aspects of the stability of singly- and multiply-charged fullerenes, i.e. the quantitative study of various unimolecular decay channels (monomer evaporation, sequential decay reactions, charge separation reactions, etc.) and, based on the measured properties, to (ii) a discussion of the possible decay mechanisms.

## 2. Experimental

The present measurements were carried out with a double-focusing, sector-field mass spectrometer of reversed Nier–Johnson geometry with a maximum mass resolution of 25000 and a mass range of 10000 amu at a nominal acceleration voltage of 3000 V. Figure 2 shows schematically the experimental set-up. The purified fullerene powder ( $C_{60}$  or  $C_{70}$ ) was evaporated in a temperature-controlled oven [33] (with typical temperatures between 800 and 900 K) and introduced as an effusive beam via a small orifice into the modified Nier-type ion source [45–47] of the mass spectrometer. After entering the open ion source (typical  $C_{60}$  pressure of several  $10^{-6}$  Pa) the  $C_{60}$  (or  $C_{70}$ ) beam is crossed at right angles by an electron beam with electron currents of approximately 10  $\mu\text{A}$  in the case of cross-section measurements. The electrons are guided by a weak magnetic field and can have energies varying from close to 0 up to 1000 eV with an energy spread of approximately 0.5 eV. The ions

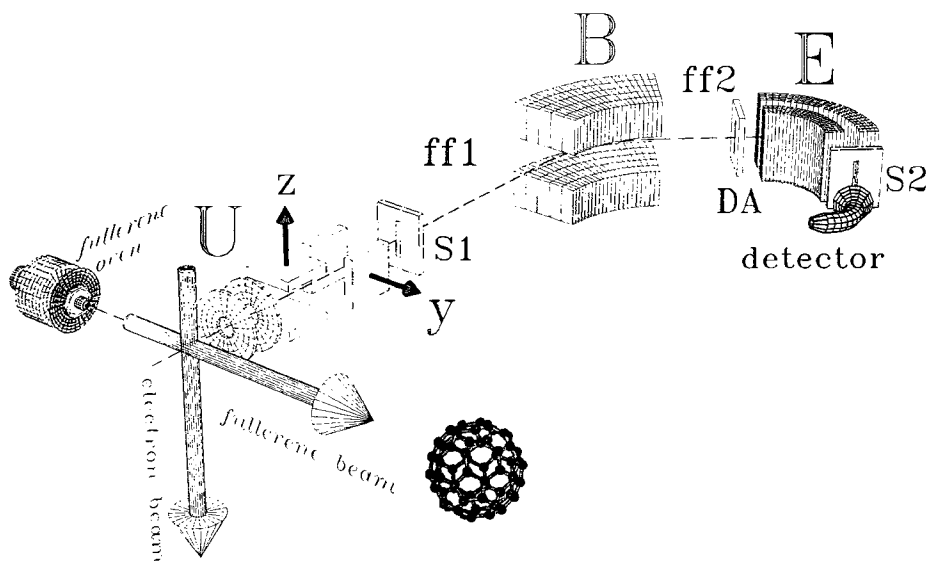


Figure 2. Schematic view of the experimental set-up including the fullerene oven, electron impact ion source and two-sector field mass spectrometer: S1, mass spectrometer entrance slit; ff1, first field-free region; ff2, second field-free region; DA, defining aperture; S2, mass spectrometer exit slit;  $U$ , accelerating voltage; B, magnetic field; E, electric field.

produced by the two interacting beams are extracted at right angles to these beams by a weak electric field. The extracted and focused ions are accelerated by an accelerating voltage of  $U = 3$  kV and after entering the mass analyzer through slit S1 are analysed by the two-sector field instrument and detected after post-acceleration by an electron multiplier and an ion counting unit controlled by a computer.

Because highly-charged fullerene ions are produced in sufficient numbers only via multiple-electron collision processes [25, 36], it was necessary for the production and study of highly-charged ions to use, besides high energy electrons (around 200 eV), high electron currents (up to 1 mA). The high electron current on the one hand increases the probability of multiple electron collisions and on the other hand creates a negative space charge strong enough to trap the ions for a sufficient time to promote these multiple collisions. Moreover, in order to increase the trapping time of the ions in the negative space charge region of the electron beam a stronger magnetic guiding field has been used and all lenses in the ion source had to be optimized to reduce the extracting field. It is interesting to note that under these experimental conditions, the ion source is operating in a similar mode as in instruments known as electron beam ion trap (EBIT) used for the study of highly-charged ions [48].

The ion source chamber is evacuated with a  $500 \text{ l s}^{-1}$  turbo molecular pump, is sealed with gold and copper rings and can be heated up to 600 K. Therefore, the residual gas pressure is below  $10^{-6}$  Pa and consists mainly of nitrogen and oxygen. Even with the effusive fullerene beam (at a typical oven temperature of 890 K) the pressure in the ion source is less than  $2 \times 10^{-6}$  Pa. It is very important to achieve this high vacuum, because multiply-charged ions with charge states higher than 5 have extremely high cross-sections for charge transfer to neutral components in the residual gas. Moreover, the whole analysing part of the mass spectrometer is metal sealed (with

the exception of the electrostatic analyser) and pumped with an oil-free turbo pump equipped with magnetic bearings. Therefore, the pressure from the ion source to the detector is always better than  $10^{-5}$  Pa.

Essential to the present study is the possibility of studying quantitatively spontaneous or collision-induced dissociations in the two field-free regions of the mass spectrometer. In order to record the corresponding unimolecular decay peaks in the first field-free region (length 60.2 cm) the HV-scan technique is used [49], whereby the change in kinetic energy occurring for the ensuing daughter ion is compensated for by proper tuning of the acceleration voltage  $U$ . The value  $U^*$  of the acceleration voltage of the centre of the metastable peak is related to the mass per charge ratios of the precursor ion and daughter ion,  $m_1/z_1$  and  $m_2/z_2$ , respectively, by

$$U^* = U \frac{m_1 z_2}{z_1 m_2} \quad (1)$$

with  $U$  the nominal acceleration voltage of the precursor ion. For the investigation of the decay reactions in the second field-free region (length 33.3 cm) the MIKE-scan technique [49] is used, which involves the proper tuning of the electric sector field  $E$ . A simple equation, as in the HV-scan, relates the value  $E^*$  at the centre of the metastable peak to the sector field voltage of the precursor ion  $E$  and the mass per charge ratios of the precursor ion and daughter ion, i.e.

$$E^* = E \frac{m_2 z_1}{z_2 m_1} \quad (2)$$

Finally, sequential metastable transitions  $m_1^+ \rightarrow m_2^+ \rightarrow m_3^+$  (where the first decay  $m_1^+ \rightarrow m_2^+$  occurs in the first field-free region and the ensuing fragment ion  $m_2^+$  then decays in the second field-free region to  $m_3^+$ ) may be studied by tuning both fields to the respective fragment ions, respectively [50].

### 3. Production of parent and fragment ions of $C_{60}$ and $C_{70}$

#### 3.1. Identification of the ions produced

The very first mass spectra of  $C_{60}$  vapour ionized by electrons already showed high numbers of multiply-charged fullerene ions (e.g. figure 1). Shortly after the discovery of the existence of the fullerenes by Kroto *et al.* [1] it became clear that these molecules may be ionized to states higher than  $\pm 1$ , i.e. charge states ranging between  $-2$  [7] and  $+4$  (see review in [26]) thus allowing for the first time the generation (in a simple way in any electron impact ion source) and study of molecules with more than three charges. Nevertheless, the efficiency of the production of multiply-charged fullerene ions strongly depends on the experimental conditions in the ion source, i.e. the electron energy, the electron current, the electron guiding (magnetic) field and the ion extraction field. In order to produce higher charge state ions (above charge state 4) it was necessary to change all of these ion source parameters in such a way as to increase the probability for multiple collisions of a fullerene target with the electrons (see above). Figure 3 shows as an example the normalized ion currents for singly- to septuply-charged  $C_{60}$  ions as a function of electron current measured under such conditions. From these relationships and also additional evidence concerning the appearance energies (i.e. it is possible under high electron current conditions to observe multiply-charged  $C_{60}$  ions already below their measured appearance energy [24, 26]) it was concluded [25] that highly-charged fullerene ions (above charge state 5)

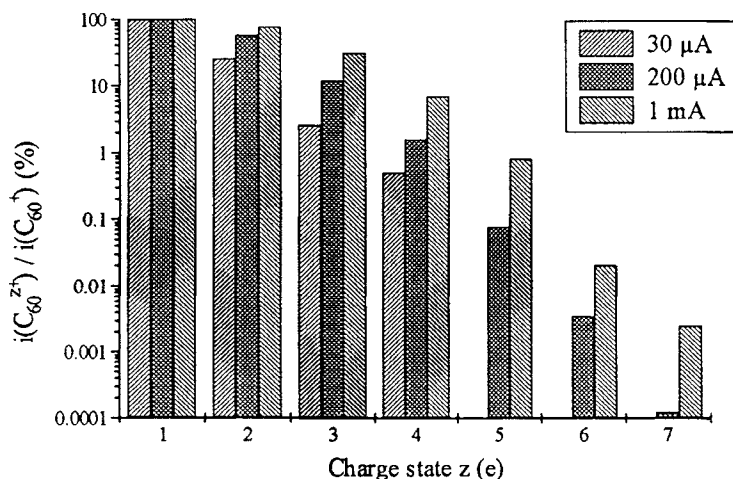
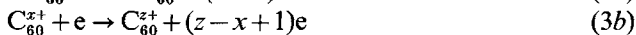
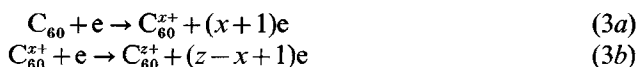


Figure 3. Normalized ion currents  $C_{60}^{z+}/C_{60}^{+}$  versus charge state  $z$  for three different electron currents (electron energy 200 eV) [25].

are produced almost exclusively by multiple-electron collision processes, i.e. stepwise ionization reactions involving at least a two-step ionization process



where the charge state  $x$  of the first reaction step is given by  $1 \leq x \leq 4$ . The occurrence of this reaction sequence is further confirmed by the fact that the highly-charged ions with charge states greater than +4 appear to be produced with an especially large probability at electron energies around 200 eV where the large cross-sections reported by Salzborn and co-workers for the electron impact ionization of fullerene ions have their respective maximum [51].

As the appearance energy of, for instance, quadruply-charged  $C_{60}$  is of the same order as the electron energy needed for producing singly-charged fragment ions (see below) the observation and identification of multiply-charged ions is usually rendered rather difficult by the existence of coinciding fragment ions. Whereas the contribution of  $C_{30}^{+}$  to  $C_{60}^{2+}$  at the mass per charge ratio of 360 amu is rather negligible due to the large abundance ratio between these two ions, peaks of more-highly-charged ions may be seriously contaminated by fragment ions having a lower charge but the same mass per charge ratio (figure 4). The only way to identify the contributions of differently charged ions which overlap each other is a careful analysis of the isotopic pattern of the peaks [22, 23, 25, 31]. Carbon consists of the two stable isotopes  $^{12}\text{C}$  and  $^{13}\text{C}$ , and therefore every cluster size has its typical peak pattern, i.e. multiply-charged carbon clusters always have signal contributions at non-integer masses (figure 4). In general the peak containing one  $^{13}\text{C}$  (the second isotopomer) can be used to identify and to determine the total abundance of the corresponding ion by summing over all the other possible isotopomers. Figure 4 shows the measured mass spectral distributions of singly- to septuply-charged  $C_{60}$  parent ions and, in comparison, calculated isotopic distributions normalized (with the exception of  $C_{60}^{6+}$  and  $C_{60}^{7+}$ ) to the measured distributions at the second isotopomer containing one  $^{13}\text{C}$ . More details of the identification of the septuply-charged parent ion  $C_{60}^{7+}$  and the existence of octuply-charged fullerene ions are given in [25] and [32, 33, 36], respectively.

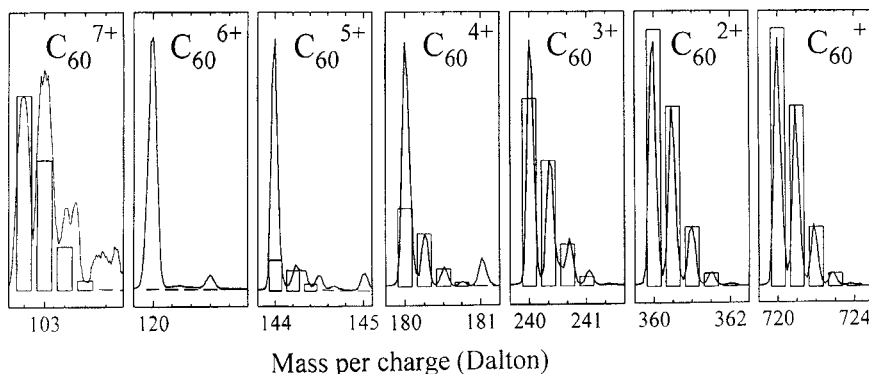


Figure 4. Measured (line graph) and calculated (bar graph) isotopic distributions for singly- to septuply-charged  $C_{60}$  ions.

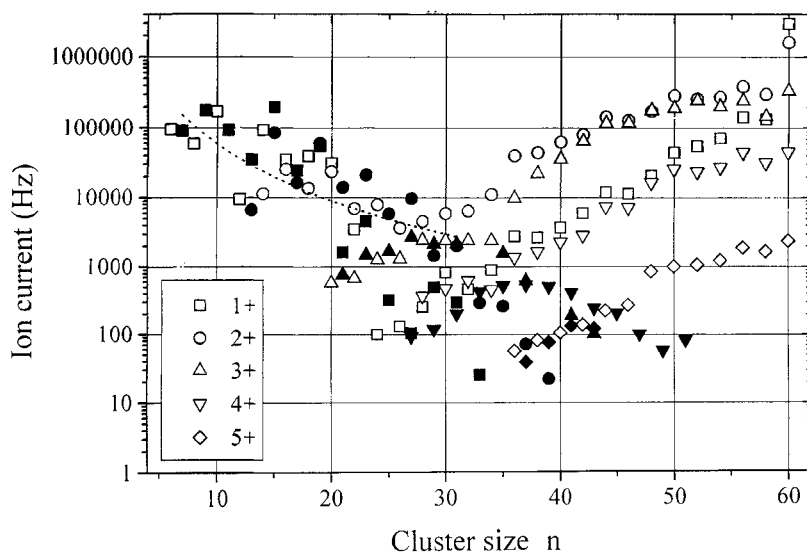


Figure 5. Isotope-corrected (see text) mass spectrum of  $C_{60}$  showing even-numbered (open symbols) and odd-numbered (filled symbols) singly-, doubly-, triply-, quadruply- and quintuply-charged ion series. Electron energy, 200 eV; electron current, 200  $\mu\text{A}$ .

Sometimes the mass resolution available at the rather weak ion currents present is not sufficient to separate coincidences. A typical example is  $C_{60}^{8+}$  which is overlapping with  $C_{50}^{5+}$ ,  $C_{40}^{4+}$ , and so on. The difference in mass between  $^{13}\text{C}^{12}\text{C}_{59}^{5+}$  and  $^{13}\text{C}^{12}\text{C}_{49}^{5+}$  is only  $\frac{1}{30}$  amu and therefore the resolution needed for the separation of these two peaks is more than 4000. This resolution cannot be achieved for the small ion signals available and therefore the measured curve in figure 4 is heavily contaminated by the fragment ions. The only chance to observe sextuply-charged ions is via sextuply-charged fragment ions or via the observation of the decay of the sextuply-charged parent ion (e.g.  $C_{60}^{6+} \rightarrow C_{58}^{6+} + C_2$ ) during its flight through the mass spectrometer (see below).

Using the above-mentioned isotope analysis an isotope-corrected mass spectrum can be obtained (figure 5), where the total signal intensity of each ion—the sum over



all isotopic peaks—is plotted versus the cluster size for different charge states. The spectrum shown in figure 5 is also corrected [46] for discrimination effects due to the kinetic energy of the fragment ions—a provision which is especially important for the smaller fragment ions, because of the relatively large kinetic energy released in their production. Several interesting features can be deduced from the results shown in figure 5.

Fragment size distributions for singly- and doubly-charged  $C_n^{z+}$  exhibit a bimodal shape with a minimum at around size  $n = 30$ . At least for singly-charged fragment ions above size 33 only even-numbered fragment ions are observed (in accordance with earlier observations), whereas below this size both even- and odd-numbered fragments are present. According to Bowers and co-workers [52] carbon cluster ions with even numbers and above size 30 can be related to three-dimensional cage structures (fullerenes), whereas smaller carbon clusters exist as chains or ring structures. The quasi-exponential decrease of the even-numbered singly- and doubly-charged fragment ions between  $n = 60$  and  $n \sim 30$  has been ascribed to sequential evaporations of  $C_2$  units [19, 53–57]. A similar dependence on  $n$  can be seen to exist for even-numbered triply-, quadruply- and quintuply-charged fragment ions, and it may be conjectured that a similar evaporation mechanism is responsible for this finding.

Whereas below the minimum at around  $n = 30$  even- and odd-numbered triply-, quadruply- and quintuply-charged fragment ion numbers are still decreasing with decreasing  $n$ , the numbers of doubly- and singly-charged fragment ions starts to increase quasi-exponentially with decreasing  $n$  at around  $n = 30$ . The conspicuous increase at lower size of the singly- and doubly-charged ions is surprising as other ordinary molecules do not show such a fragmentation pattern (i.e. the U-shaped fragment mass spectrum). Similar bimodal distributions have already been observed by Hertel, Campbell and co-workers in the case of photo fragmentation and collisional fragmentation of  $C_{60}$  [58–60], by LeBrun *et al.* [61] bombarding  $C_{60}$  with highly-charged Xe ions in the MeV range and by Gaillard and co-workers [62] for the fragmentation of mass-selected 60 keV  $amu^{-1} H_n^+$  ions induced by single collision with He atoms. Moreover, nuclear multifragmentation displays very similar features (e.g. for nuclear fragments emerging from heavy nuclei bombarded by GeV protons [63]). The fall-off at small masses has been described in some of these earlier studies by a power-law. In analogy to these cases, the present experiment may also be interpreted by a power-law for the size  $n$  of singly- and doubly-charged carbon cluster ions  $C_n^{z+}$  (with  $n \leq 30$ ) proportional to  $n^{-x}$ , where  $x \sim 2.6$ . This behaviour is similar to the case of nuclear fragmentation [64], where  $x \sim 2.6$  in inclusive (impact parameter integrated) reactions; to the hydrogen cluster ion case [62], where  $x \sim 2.63$ ; and to the  $C_{60}$  multifragmentation experiment of LeBrun *et al.* [61], where  $x \sim 1.3$ . In the case of nuclear multifragmentation reactions the power-law arises as a consequence of the finiteness of the system and of the integration over various excitation energies [63]. Further experiments are needed to clarify the underlying reaction mechanism of the present electron impact induced pattern at the low mass side of the distribution (some preliminary results on this subject are given in [37]).

It is interesting to point out that at least for odd-numbered doubly-, triply- and quadruply-charged fragment ions the fall-off discussed above appears to be continued beyond the minimum point in the U-shaped distribution (see the general trend of the filled symbols in figure 5) and that therefore odd-numbered carbon cluster ions exist above the previously observed size limit of the singly-charged ion at size 33 (the largest odd-numbered carbon cluster ion in the present study is  $C_{51}^{4+}$ ). This again would

indicate that these odd-numbered ions may exist in a different structure than their even-numbered counterparts at around the same size. In further experiments we hope to identify the structure and production mechanism of these large odd-numbered highly-charged carbon cluster ions.

Finally, the relative abundance of multiply-charged parent  $C_{60}$  ions is remarkably high and the abundance of doubly- and triply-charged fragment ions is even higher than that of the corresponding singly-charged fragments. This is in accordance with recent accurate partial ionization cross-section measurements for these ions [30, 38] described below. In contrast to the data in figure 5, which were taken at very high electron current, the cross-section measurements have been made with very low electron currents in order to assure single-collision conditions.

### 3.2. Absolute partial and total ionization cross-sections

Despite numerous measurements of mass spectral cracking patterns of  $C_{60}$  and other fullerenes [19, 43, 44], quantitative partial and total ionization cross-section functions (cross-section  $\sigma$  versus electron energy  $E$ ) for  $C_{60}$  and  $C_{70}$  are not yet available, the only exception to this being the cross-section data for attachment to  $C_{60}$  [7] and a cross-section value of  $53.5 \times 10^{-20} \text{ m}^2$  [65] for the production of the parent ion at an electron energy of 38 eV [66]. This is primarily because  $C_{60}$  and  $C_{70}$  are solid at room temperature, making it difficult to determine the absolute gas density of the fullerene target introduced into an ion source after sublimation in an oven. A knowledge of this gas density is, however, necessary for the determination of the absolute cross-sections from the measured ion currents produced by the interaction of a beam of electrons (of known current and energy) with the fullerene gas target in an ion source.

Recently we were able to carry out the first measurements of cross-section functions for the production of the various parent ions  $C_{60}^{z+}$  and the most abundant fragment ions  $C_{60-2m}^{z+}$  ( $m = 1 \dots 8$ ) by single electron collision in the energy range from threshold up to 1000 eV, including ions with charge states up to  $z = 4$  and fragment ions down to  $C_{44}$  [30]. For these measurements we used the crossed beams apparatus described above invoking, however, for these measurements a novel technique for the absolute calibration of the cross-sections (see below). The relative partial ionization cross-section functions for  $C_{60}$  cations have been obtained following the procedures outlined previously [45–47, 67] to obtain reliable cross-section data, i.e. using electron currents below 10  $\mu\text{A}$  and taking into account discrimination effects in the ion source extraction procedure and during the flight through the mass analyser, by using the penetration field extraction and deflection mass spectrometry technique, respectively. The electron energy scale was calibrated using known cross-section curves for the production of  $\text{SF}_6$  anions and the known onsets for partial cross-sections for the rare gases. These other gases are introduced into the ion source via supplementary gas inlets.

In order to calibrate the measured relative partial ionization cross-sections for the various  $C_{60-2m}^{z+}$  ions a novel technique has been employed, because the conventional relative flow methods used for ordinary gas targets [18, 68] cannot be applied here. The key to the present technique lies in the fact that the interaction of electrons with  $C_{60}$  leads to both negative and positive ions and that we have recently been able to measure the absolute attachment cross-section function for the production of  $C_{60}^-$  using a combination of crossed beams and flowing afterglow/Langmuir probe techniques [7, 9, 12]. Therefore, measurement of the  $C_{60}^-$  and  $C_{60}^+$  ion yield under identical ion

source (and mass spectrometer) conditions (gas pressure, electron currents, ion extraction and detection efficiency) should allow us to derive the absolute ionization cross-section for the production of  $C_{60}^+$ . As the ion extraction and detection efficiency is, however, usually different for positive and negative ions (in particular in the case of different electron energies considered), these efficiencies have been determined in the present case using a calibrant gas and corresponding ions for which both the attachment and the ionization cross-sections are known. Measuring the production of  $SF_4^+$  and  $SF_4^-$  via electron interaction with  $SF_6$  under exactly identical experimental conditions as the formation of the respective  $C_{60}$  ions we obtain the necessary correction factor from the ratio of the measured ion currents and the known cross-sections [69, 70]. It transpires that the total detection efficiency for the negative ions is approximately a factor of 10 smaller than that for the positive ions and is strongly dependent on the experimental conditions used.

The cross-section thus derived for the production of  $C_{60}^+$  is  $(22 \pm 8) \times 10^{-20} \text{ m}^2$  at an electron energy of 100 eV (see also a more accurate value of  $24.6 \times 10^{-20} \text{ m}^2$  given in [38]) and thus lies way below the previous determination using a Knudsen cell approach [65]. The error bars given correspond only to the statistical uncertainty and do not include errors in the cross-sections used in the calibration procedure and other systematic errors (a conservative estimate of these uncertainties leads to a factor of two in the overall error). The other partial ionization cross-section functions of  $C_{60}$  can be derived from the measured relative partial ionization cross-sections, and the total counting or total ionization cross-sections can be obtained from the ordinary or charge-weighted sum of all the partial cross-sections, respectively. This is the first time that this procedure has been used, but it has obvious value for the quantitative study of electron impact ionization of other normally solid substances such as some polycyclic aromatic hydrocarbons, a topic of current interest in mass spectrometry [71] and astrochemistry [72].

The partial ionization cross-section results obtained for the parent ions  $C_{60}^+$  to  $C_{60}^{4+}$  and the two strongest fragment ions are presented in figure 6. By far the largest cross-section is observed for the parent ion  $C_{60}^+$ . Although this is in contrast to the known situation for ordinary larger polyatomic molecules (where the parent ion is usually almost non-existent [5, 18], with the exception of some polycyclic aromatic hydrocarbons [73]), it is nevertheless in accordance with previous mass spectrometric studies and theoretical considerations (RRKM calculations) of the ionization and fragmentation of  $C_{60}$  [19]. The large binding energy and the large number of degrees of freedom (and the resulting huge kinetic shift of more than 34 eV) render dissociative ionization processes of  $C_{60}$  less likely. The maximum value for the process  $C_{60} \rightarrow C_{60}^+$  of  $22 \times 10^{-20} \text{ m}^2$  is close to the value of  $21 \times 10^{-20} \text{ m}^2$  reported previously [51] for the process  $C_{60}^+ \rightarrow C_{60}^{2+}$ . This is not surprising taking into account that the HOMO level  $h_u$  of the neutral molecule is tenfold degenerate [74] and that the removal of the first two  $\pi$  electrons requires rather similar ionization energies of 7.6 and 11.4 eV [24], respectively. In contrast, the maximum cross-section for the process  $C_{60}^+ \rightarrow C_{60}^{4+}$  which requires a much larger ionization energy of 27.4 eV [24] is only  $13 \times 10^{-20} \text{ m}^2$  [51].

Another interesting anomaly is the rather large magnitude of the cross-section for the production of multiply-charged *parent* ions relative to that of the singly-charged parent ion (figure 6). Whereas here the ratio for doubly- to singly-charged is more than 20%, for ordinary molecules or atoms this ratio is seldom more than a few percent (the gas with the highest percentage of doubly-charged ions known so far is xenon with approximately 12% [75]). The reason for these enhanced production cross-sections

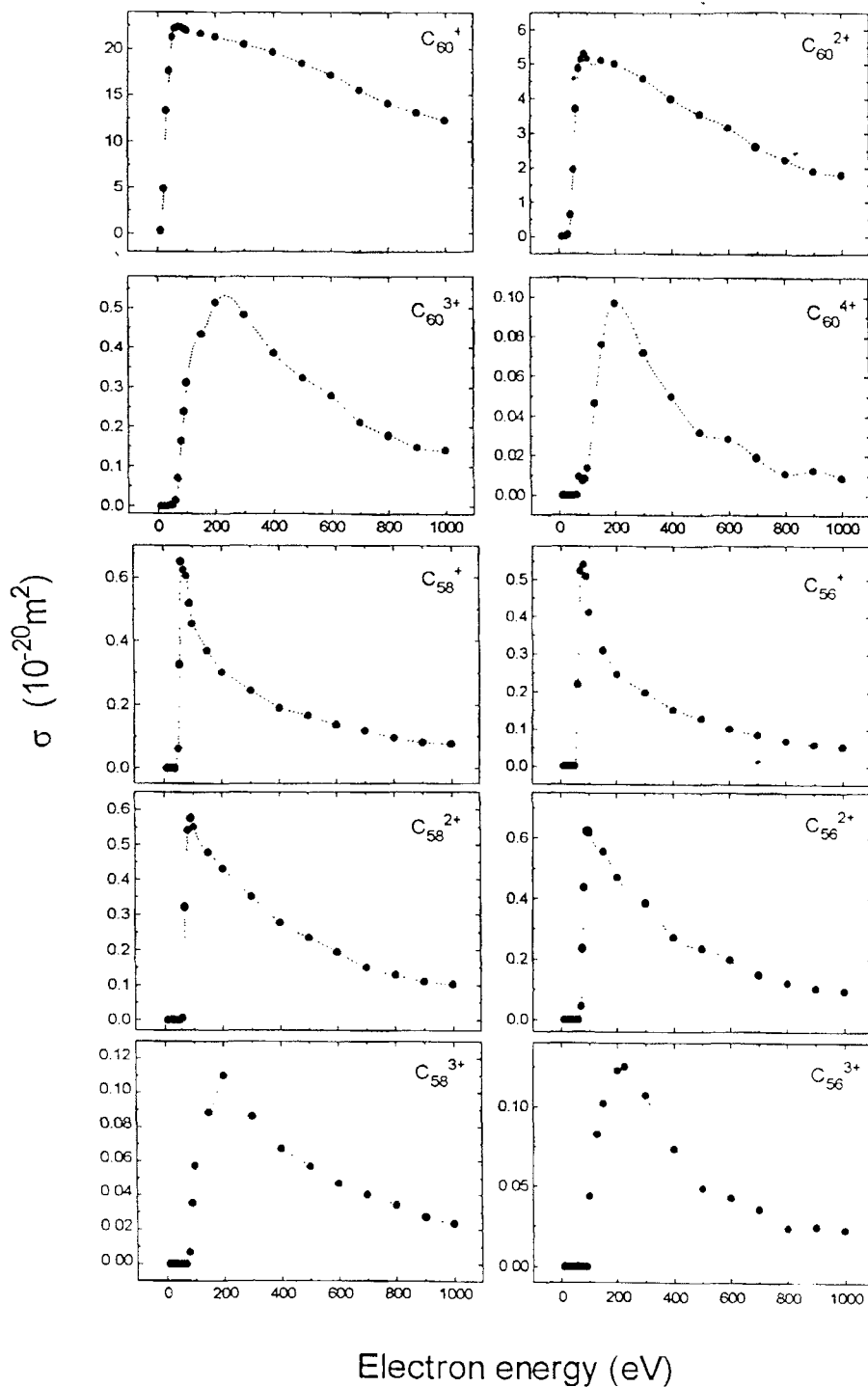


Figure 6. Absolute ionization cross-section versus electron energy for the formation of singly-, doubly-, triply- and quadruply-charged  $C_{60}$  parent ions and for the formation of the singly-, doubly- and triply-charged fragment ions  $C_{58}^{z+}$  and  $C_{56}^{z+}$ .

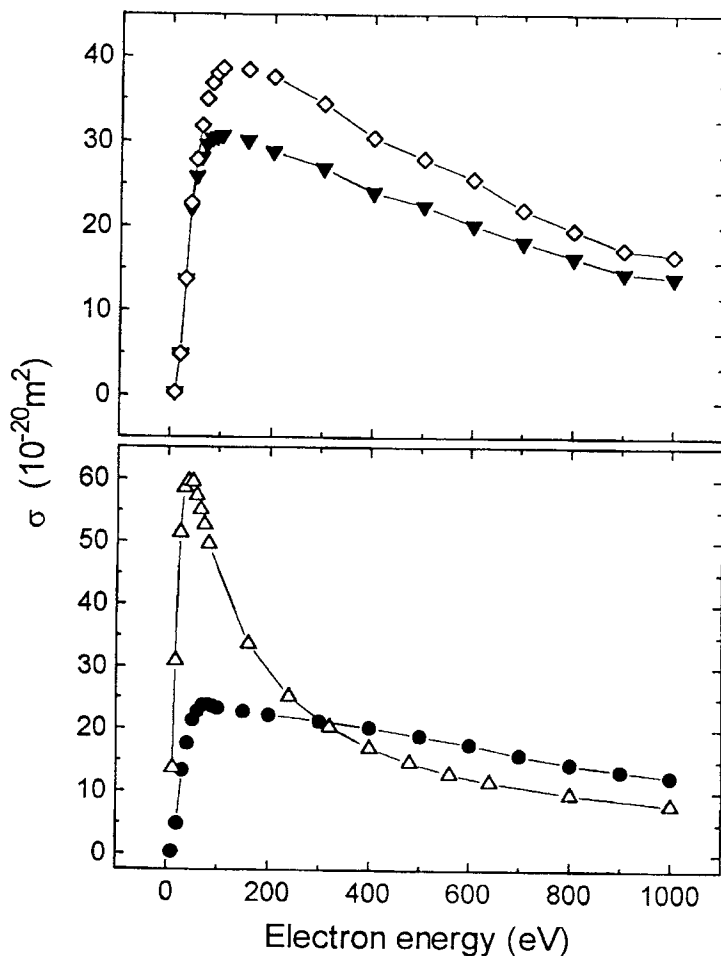


Figure 7. Absolute total ionization cross-section ( $\diamond$ ) and total counting cross-section ( $\nabla$ ) versus electron energy for  $\text{C}_{60}$  (upper part). In the lower part the sum of the measured cross-sections for the production of singly-charged ions of  $\text{C}_{60}$  ( $\bullet$ ) is compared with calculated values ( $\triangle$ ) using a semi-classical approach similar to that described in [78].

lies on the one hand in the fact that the production of doubly- and triply-charged ions is energetically more favourable than the production of fragment ions (the appearance energy of  $\text{C}_{60}^{2+}$  and  $\text{C}_{60}^{3+}$  lies below that of any fragment ion of  $\text{C}_{60}$  [24]). In addition the sheer size of  $\text{C}_{60}$  and the fact that a secondary electron from an initial single-ionization process may be ejected into the empty centre of the cage and subsequently interact anew with the electron shell of the  $\text{C}_{60}$  enhances the chances of inelastic multiple-electron collisions within this quantum system, thereby increasing the probability of the production of multiply-charged ions. Similar effects have been observed for the production of multiply-ionized van der Waals clusters [76] and metal clusters [77]. This also explains the anomalous situation encountered in the case of the *fragment* ion cross-sections depicted in figure 6, where the maximum values for doubly-charged ions is of the same magnitude as that of the respective singly-charged ion.

The absolute total ionization and total counting cross-sections are given in figure 7 (upper part). In the lower part of figure 7 we have plotted the sum of all single

ionization cross-sections. This quantity has been calculated using a simple version of the Deutsch–Märk (DM) approach [78] based on a combination of binary encounter approximation and the Born–Bethe approximation. There appears to be good agreement between the experimental data and the predicted values for energies above 200 eV. Whereas this semi-classical approach takes into account the special geometry of the  $C_{60}$  molecule, the simple additivity rule approach [79] (assuming  $sp^2$  hybridization) gives a measure for the total counting ionization cross-section at an electron energy of 70 eV of approximately  $103 \times 10^{-20} \text{ m}^2$  which is much higher than the present value of  $30 \times 10^{-20} \text{ m}^2$  and the simple geometric cross-section of  $38\text{--}78 \times 10^{-20} \text{ m}^2$  (the lower limit corresponding to the cage radius and the upper limit to the hard sphere radius of  $C_{60}$ ). It is interesting to note that the one previous calibration [65]—using a Knudsen cell approach—leads to total counting cross-sections which are also larger than these geometric cross-sections. A more detailed account of the measured  $C_{60}$  cross-sections and also of those of  $C_{70}$  will be presented in [38] (see also [30]).

#### 4. Appearance energies, breakdown curves and binding energies

##### 4.1. Appearance energies

One of the interesting properties to be determined from electron impact ionization cross-section measurements are the threshold values for the appearance of the various ions providing information on the energetics of the ionization process [80]. For ordinary molecules this has so far been possible only for singly- and doubly-charged parent and fragment ions [81], whereas in this case it is the first time that appearance energies can be determined for ions with higher charge states (the results for charge states up to 3 have been recently summarized in table 1 of [26]). For singly- and doubly-charged  $C_{60}$  ions ionization energies were measured with different methods and the values of 7.64 for  $C_{60}^+$  [82] and 11.43 for  $C_{60}^{2+}$  [83] are well-established today. For  $C_{60}^{3+}$  the reliable (see discussion in [26]) ionization energies so far determined include the charge stripping result of 17.0 eV by Lifshitz *et al.* [84], the corrected charge transfer bracketing results of 15.7 and 15.6 eV by McElvany *et al.* [43] and Javahery *et al.* [85], respectively, and our own electron impact ionization result [26] of 16.6 eV. Moreover, we also measured the appearance energies for singly-, doubly- and triply-charged  $C_{60}$  fragment ions and compared these data with results for singly-charged fragment ions reported by Anderson and co-workers [86] using a charge- and energy-transfer fragmentation technique. Recently we extended these earlier studies to (i) singly-, doubly- and triply-charged parent and fragment ions for  $C_{70}$  and (ii) ionization energies for quadruply-charged fullerene ions including the parent ions  $C_{60}^{4+}$ ,  $C_{70}^{4+}$  and the fragment ions  $C_{58}^{4+}$ ,  $C_{56}^{4+}$  from  $C_{60}$  and  $C_{68}^{4+}$ ,  $C_{66}^{4+}$ ,  $C_{64}^{4+}$  and  $C_{62}^{4+}$  from  $C_{70}$ , respectively [24]. As (i) all the quadruply-charged fullerene ions may overlap with doubly-charged carbon cluster ions and as (ii) the even-numbered quadruply-charged ions may in addition coincide with singly-charged carbon cluster ions, some of these appearance energy measurements had to be made using the respective isotopomer ion containing on  $^{13}\text{C}$  atom in order to exclude possible coincidences with contaminating lower-charged ions. Thus the mass resolution for these appearance energy measurements was set to approximately 1000 in order to clearly distinguish isotopic peaks containing one  $^{13}\text{C}$  atom from peaks containing only  $^{12}\text{C}$  atoms. Moreover, the electron current was set below 50  $\mu\text{A}$  in order to prevent space charge effects in the ion source and extraction region and in particular multiple electron collisions during the ionization

Table 1. Appearance energies (in eV) for singly-, doubly-, triply- and quadruply-charged parent and fragment ions of  $C_{60}$  and  $C_{70}$ , respectively [24, 26].

$C_{60-2m}^{z+}$				
$m$	$z = 1$	$z = 2$	$z = 3$	$z = 4$
0	$7.6 \pm 0.5$	$19 \pm 0.5$	$35.6 \pm 1$	$63 \pm 2$
1	$43.7 \pm 1.5$	$54 \pm 2$	$70.3 \pm 2.2$	$92 \pm 3.5$
2	$48.8 \pm 1.6$	$59.8 \pm 1.9$	$76 \pm 2$	$95 \pm 4.4$
3	$54.3 \pm 2$	$65.1 \pm 2.4$	$82.2 \pm 3.1$	$108 \pm 5$
4	$59.9 \pm 2.1$	$71.8 \pm 3.3$	$90.6 \pm 4.1$	
5	65	75.8	94.1	
6	73.4	82.1		
7	78.7	86.1		
8	85.1			

$C_{70-2m}^{z+}$				
$m$	$z = 1$	$z = 2$	$z = 3$	$z = 4$
0	$8 \pm 0.5$	$19.4 \pm 0.7$	$34.9 \pm 1.5$	$62.5 \pm 2$
1	$49.4 \pm 1.4$	$61.5 \pm 1.6$	$73.9 \pm 2.3$	$94 \pm 3.8$
2	$54 \pm 1.7$	$66.1 \pm 2$	$79.9 \pm 2.6$	$100 \pm 4.1$
3	$59.5 \pm 1.9$	$71.8 \pm 2.8$	$85.2 \pm 2.9$	$105 \pm 5.2$
4	$64.6 \pm 2.2$	$76.2 \pm 3.5$	$90.5 \pm 3.9$	$112 \pm 4.8$

process (see the discussion in [25] and [87]). The electron energy scale was calibrated with the help of measured ionization efficiency curves of singly- and doubly-charged Ar or Ne ions using  $z$ th root extrapolation to the respective appearance energies [88, 89].

For  $C_{60}$  and  $C_{70}$  a whole series of ionization efficiency curves were measured for all singly- and multiply-charged (up to quadruply-charged) parent and fragment ions down to  $C_{46}^{z+}$  and  $C_{62}^{z+}$ , respectively. It was not possible to measure  $C_{60}$  as a fragment ion from  $C_{70}$ , because (i) the main impurity in the  $C_{70}$  sample is  $C_{60}$  and in addition (ii) small traces of  $C_{60}$  came from the vessel walls as a residual background and memory effect from earlier measurements. Table 1 gives all appearance energies determined from the measured ionization curves of these ions.

As the ionization efficiency curves for fullerene ions—even for the singly-charged parent ions (figure 8 shows as an example the respective data for the  $C_{60}$  parent ions)—are strongly curved close to the onset, it is rather difficult to determine the appearance energy in the usual way by extrapolating the data points back to the  $x$ -axis (see for example the ionization curves shown on the left side of figure 8). Using a special threshold extrapolation procedure [26] we raised the original data points to a certain power ( $\frac{1}{p}$ ) in order to linearize the lower part of the ionization efficiency curve over at least 10 eV (see the linearized ionization curves shown on the right side of figure 8). For these fullerene ions the power ( $p$ ) had to be chosen considerably larger than in the case of atomic ions which follow a  $z$ th power-law with the charge state  $z$  [88, 89]. The reason for this is the large number of electronic and vibrational states of the fullerene ions which can be populated by electron impact ionization. Each state itself should obey the power-law of the charge, but the sum over all of these states gives an additional curvature. This strongly curved onset of the ionization efficiency curve not

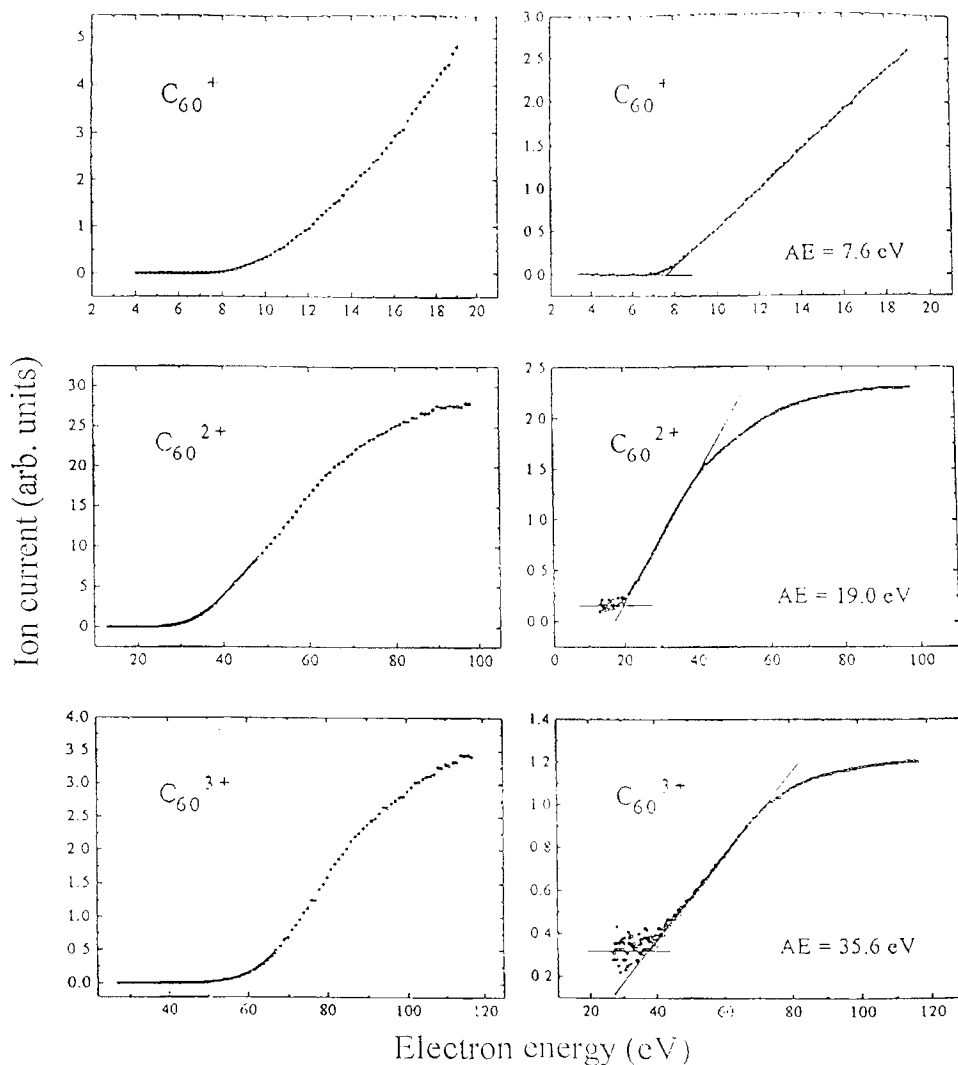


Figure 8. Ionization efficiency curves for the electron impact induced production of  $C_{60}^+$ ,  $C_{60}^{2+}$  and  $C_{60}^{3+}$  (left hand side) and the same data sets modified by a  $\frac{1}{p}$  power-law (with an exponent  $p$  of 1.67, 4 and 6.7, respectively) in order to linearize the threshold region (right hand side). The lines shown (right hand side) represent the fitted linear regression allowing an easy determination (see text) of the appearance energy  $AE$ .

only exists in the case of electron impact ionization but also limits the accuracy of the determination of appearance energies via photon-ionization of  $C_{60}$ . More information about the present evaluation method is given in [24, 26].

Figure 9 shows the appearance energies of the parent and fragment ions of  $C_{60}$  (filled symbols) compared with those of  $C_{70}$  (open symbols). The appearance energies of the fragment ions of both fullerenes exhibit a linear relationship with the number of lost  $C_2$  units to a remarkable degree. A similar result (with the exception of  $C_{52}^+$ ) has been reported by Anderson and co-workers [86] for appearance energies for singly-charged  $C_{60}$  fragment ions obtained by studying collisions between  $Ne^+$  and neutral  $C_{60}$  as a function of ion energy. These results indicate that the energy necessary to



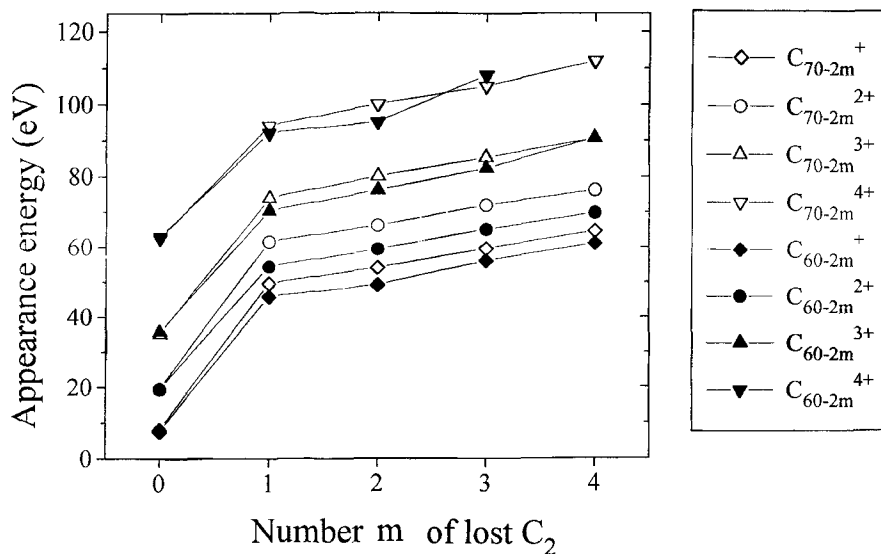


Figure 9. Appearance energies of singly-, doubly-, triply- and quadruply-charged ions produced by electron impact ionization of  $C_{60}$  (filled symbols) and of  $C_{70}$  (open symbols) as a function of the number of  $C_2$  units lost in the ionization process [24, 26].

remove an additional  $C_2$  unit from a fragment ion is approximately constant. As this energy is also independent of the charge state (all curves have the same slope), we conclude that there is a common underlying statistical process for the evaporation of a  $C_2$  unit independent of the charge state or precursor size of the dissociating ion once the first fragment ion has been produced.

Moreover, whereas the additional energy to remove a further  $C_2$  unit from a fragment ion is in the order of  $5.7 \pm 1.3$  eV (and may be related to the relative binding energies via statistical models, see below), the energy to remove such a  $C_2$  unit from the parent ion is, in the case of  $C_{60}$ , approximately 36 eV. This huge kinetic shift is caused by the many degrees of freedom and the rather large binding energy  $BE(C_{58}^+ - C_2)$  of  $7.1 (\pm 0.4)$  eV determined recently by Foltin *et al.* [19] from the electron impact cross-section threshold behaviour of the first fragment ions using RRKM and FHBT theory (see below). In this context it is interesting to note that the appearance energy of all the fragment ions of  $C_{70}$  lie consistently above the corresponding fragment ions of  $C_{60}$  losing the same number of  $C_2$  constituents (figure 9). In contrast the appearance energies for the mother ions  $C_{60}^{z+}$  and  $C_{70}^{z+}$  are more or less the same within the error limits. Although the difference between the appearance energies of the corresponding fragment ions of  $C_{60}$  and  $C_{70}$  in most of the data points is smaller than the uncertainty of the values, the general trend that the appearance energy points of the  $C_{70}$  fragment ions lie above those of the  $C_{60}$  fragment ions is statistically significant, because it occurs for all charge states and almost all fragment ion sizes. The reason for this difference can be ascribed to the much larger number of degrees of freedom of  $C_{70}$ , thereby causing a larger kinetic shift in the appearance energy of the fragment ions.

A further interesting result to be deduced from figure 9 concerns the behaviour of the ionization energy of the parent fullerene ions versus final charge state (up to charge state 4). Recent theoretical investigations by Yannouleas and Landman [74] based on a new local density approximation (LDA) method including (i) a stabilized jellium

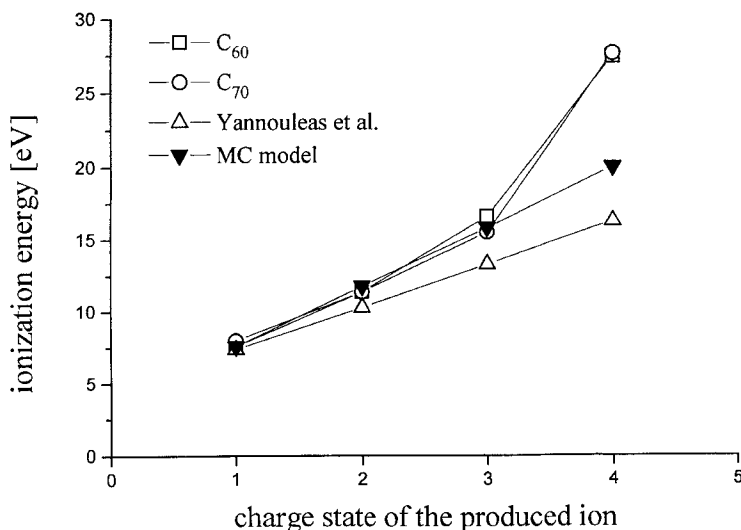


Figure 10. Ionization energy versus final charge state  $z$  for  $C_{60}$  (open circles) and  $C_{70}$  (open triangles) parent ions derived from the respective appearance energies given in table 1. Also shown for comparison are theoretical predictions by Yannouleas and Landman [74] using a new LDA method (open squares) and predictions [24] by the molecular capacitance model (filled triangles).

approximation, (ii) a shell correction method and (iii) the effect of icosahedral symmetry, predict that the ionization energy for  $C_{60}$  (similar predictions for large aromatic hydrocarbons using the molecular capacitance model are given in Smith [90]) should exhibit a linear relationship with the final charge state  $z$ . Figure 10 shows the ionization energies for  $C_{60}^{z+}$  and  $C_{70}^{z+}$  (with  $z$  the final charge state from 1 to 4) versus  $z$ . The open squares are the values predicted by Landman and co-workers for  $C_{60}^{z+}$ , the filled triangles are the predictions from the molecular capacitance model and the open circles and triangles are the experimental values deduced from figure 9 for  $C_{60}$  and  $C_{70}$ , respectively. It is important to note that the data presented here are in good agreement with previous reliable determinations on  $C_{60}$  including data up to charge state 3 (using photoionization [82, 83, 91, 92], charge stripping [84, 93] and corrected charge transfer [85, 94] techniques). Moreover, see also recent data [40] up to charge state  $z = 6$ .

#### 4.2. Breakdown curves and binding energies

One of the most intriguing properties of  $C_{60}$  is its particular stability against unimolecular fragmentation upon electron impact ionization. Many investigations have been devoted to this subject (summarized recently in [44]) and it is commonly accepted today that the dominant fragmentation mechanism involves the (sequential) loss of  $C_2$  units from the energized  $C_{60}^{++*}$ . Despite the large number of studies performed, the energetics of the simple dissociation reaction



is still in question, i.e. there exist values ranging from approximately 4 up to 12 eV as determined by electron impact ionization, photoionization, collision resilience experiments and theoretical studies (a summary of the various binding energy values

Table 2. Activation energies  $E_a$ , derived from measured appearance energies with the help of formulae (5) for  $E(k)$ , see text.

Fragmentation channel	$E_a$ (eV) (5a) $\equiv$ (5b)
$C_{60}^+ \rightarrow C_{58}^+ + C_2$	7.06
$C_{58}^+ \rightarrow C_{56}^+ + C_2$	6.78
$C_{56}^+ \rightarrow C_{54}^+ + C_2$	6.60
$C_{54}^+ \rightarrow C_{52}^+ + C_2$	6.46
$C_{52}^+ \rightarrow C_{50}^+ + C_2$	6.27
$C_{50}^+ \rightarrow C_{48}^+ + C_2$	6.57
$C_{48}^+ \rightarrow C_{46}^+ + C_2$	6.39
$C_{46}^+ \rightarrow C_{44}^+ + C_2$	6.39

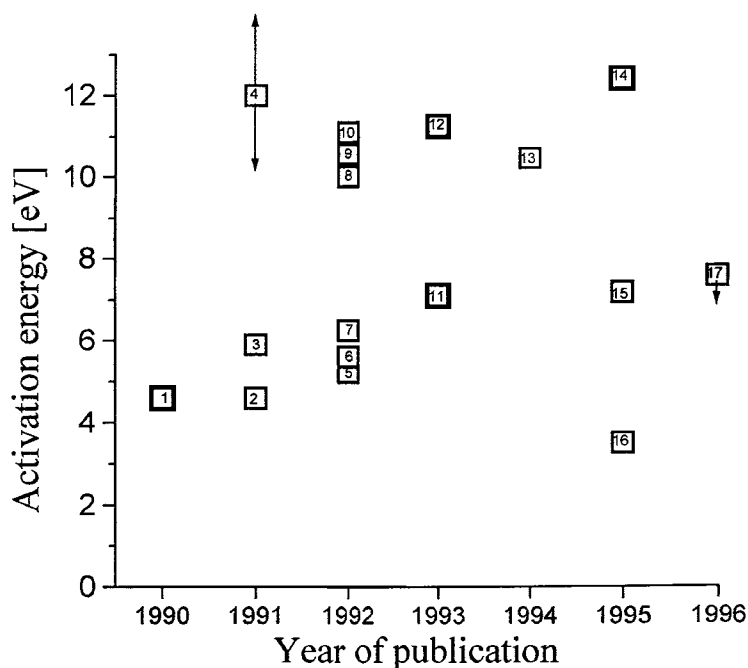


Figure 11. Activation energy for the decay reaction  $C_{60}^+ \rightarrow C_{58}^+ + C_2$  as determined by theoretical (9, [100]; 10, [101]; 12, [102]; and 13, [103]) and experimental (1, [55]; 2, [56]; 3, [95]; 4, [96]; 5, [97]; 6, [98]; 7, [92]; 8, [99]; 11, [19]; 14, [104]; 15, [105]; 16, [106]; and 17, [34]) studies.

is reported in figure 11). Some preference has been given to the value of  $7.1 \pm 0.4$  eV reported by Foltin *et al.* [19] based on a comparison between measured and calculated (using RRKM [107] and FHBT [95]) breakdown curves. As the only free parameter in these calculations is the choice of the transition state, we have recently [34] repeated these calculations with transition states of varying tightness (see below) yielding an upper limit for the binding energy of approximately 7.6 eV.

Laskin and Lifshitz [108] have also recently discussed the energetics of sequential  $C_2$  evaporations using two models—the magic shell and the magic number model—to interpret by RRKM calculations their metastable fraction measurements. Their results appear to favour the magic shell model (as already predicted by Klots [95] on

the basis of metastable fraction data by Bowers and co-workers [55]). To shed more light on this interesting question we have recently extended [34] those earlier studies by taking a new route to determine the consecutive binding energies, i.e. first relating the measured appearance energies of the fragment ions, with the help of FHBT calculations, to the respective binding energies and then using these binding energies to calculate with the help of RRKM considerations the breakdown curves for these fragment ions. Agreement between these calculated breakdown curves and the measured ones should lend credence to the binding energies thus derived.

Following the suggestions of the finite heat bath theory [95] we calculated the activation energies,  $E_a$ , for successive  $C_2$  evaporations from  $C_{60}^+$  using the respective fragment ion appearance energies (given in table 1). The energy of an isolated molecule,  $E(k)$ , and the temperature,  $T_b$ , in a heat bath that gives the same value of the rate constant,  $k$ , are related by

$$E(k) = E'(T_b) - k_B T_b + \frac{E_a}{2} + \frac{E_a^2}{12C \cdot k_B T_b} + \dots \quad (5a)$$

where  $C$  equals the heat capacity minus one (in units of  $k_B$ ) and  $E'(T_b)$  is the canonical energy of the parent ion at the temperature  $T_b$ . On the other hand the energy of the molecule that evaporates a  $C_2$  unit is given by:

$$E(k) = AE(\text{daughter ion}) + E'(T_{\text{oven}}) - IE(C_{60}) - \sum E_a(\text{previous evaporations}) \quad (5b)$$

where  $AE$  is the measured appearance energy of the daughter ion (table 1),  $E'(T_{\text{oven}})$  is the canonical energy of  $C_{60}$  at the given temperature of the oven in which the  $C_{60}$  powder is evaporated (890 K in this experiment) and  $IE = 7.6$  eV, the ionization energy of  $C_{60}$  [82]. Assuming an activation energy  $E_a = 7.06$  eV [19] for the reaction (4) we can vary  $T_b$  until (5a)  $\equiv$  (5b) and thus arrive at a Gspann parameter  $\gamma = E_a/k_B T_b \cong 25.6$ , which is in very good agreement with previous determinations of  $\gamma$  (see below). Assuming further that  $\gamma$  is constant we can deduce the activation energies for subsequent evaporation reactions  $C_{58}^+ \rightarrow C_{56}^+ + C_2$ ,  $C_{56}^+ \rightarrow C_{54}^+ + C_2$ , ...  $C_{46}^+ \rightarrow C_{44}^+ + C_2$ , simply by varying  $T_b$  until (5a)  $\equiv$  (5b).

The results obtained for the successive binding energies are summarized in table 2. It can be seen that the activation energy for the reaction (4) is higher than that for all further fragmentations and that the relative decrease with decreasing cluster size is rather small and of similar magnitude. One exception is the reaction  $C_{50}^+ \rightarrow C_{48}^+ + C_2$  which seems to have a significantly higher activation energy than its precursor reaction. Thus the fact that the binding energies decrease only slightly between  $C_{60}^+$  and  $C_{46}^+$  supports the magic shell model introduced by Laskin and Lifshitz [108].

To check the consistency of the calculated binding energies with experimental data, we have used these binding energies to compute the breakdown graph of  $C_{60}$  and have compared the calculated breakdown graph with experimental breakdown curves. The RRKM method used has been described in detail in our previous paper [19]. The present procedure involves three steps, i.e. (i) conversion of the measured ionization cross-section curves of the fragment ions of  $C_{60}$  to breakdown curves, (ii) calculation of theoretical breakdown curves using unimolecular fragmentation rates calculated by RRKM theory, and (iii) comparison of the peak positions and the relative peak heights in the measured and the calculated breakdown graphs (more details of the whole procedure are given in [34]).

In short, for electron energies  $E$  close to the threshold for fragmentation, the

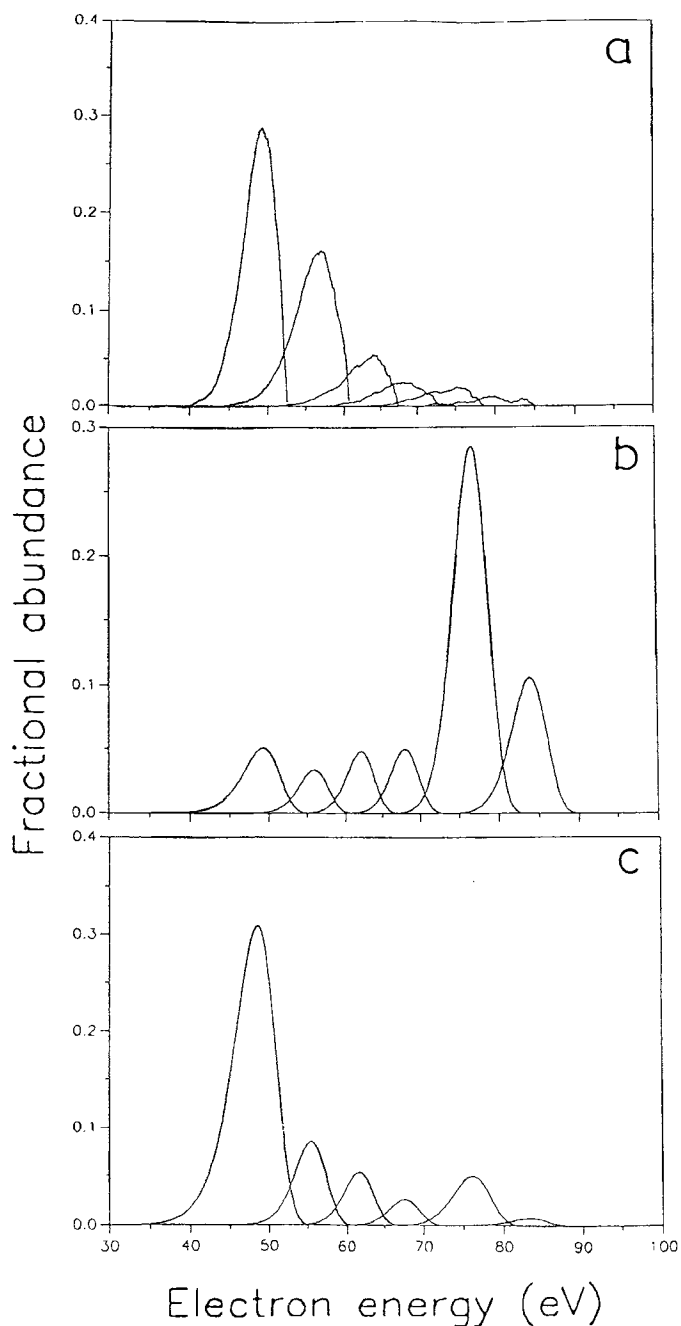


Figure 12. (a) Experimental breakdown graph obtained by taking second derivatives of the measured ionization efficiency curves for  $C_{58}^+$ ,  $C_{56}^+$ , ...,  $C_{48}^+$  fragment ions of  $C_{60}$ . (b) Breakdown graph of the  $C_{60}^+$  ion calculated with the help of RPKM for fragment ions  $C_{58}^+$ ,  $C_{56}^+$ , ...,  $C_{48}^+$  using the activation energies for successive fragmentation steps given in table 2. (c) Breakdown graph from (b) convoluted with the energy deposition function  $Kf(\epsilon) = \exp(8 \cdot 12 - 0 \cdot 129 \epsilon)$ . Results from [34].

fragment ion current  $i_m$  of the fragment ion  $C_{60-2m}^+$  is assumed to obey the linear threshold law [80], i.e.

$$i_m(E, t_1, t_2) = K \int_0^{E-E_i} \mathcal{F}_m(\varepsilon, t_1, t_2) f(\varepsilon) (E - E_i - \varepsilon) d\varepsilon \quad (6)$$

where  $K$  is an instrumental constant,  $E_i$  is the ionization energy of the  $C_{60}$  molecule, function  $f(\varepsilon)$  describes the probability per square of the unit energy to ionize  $C_{60}$  to an excited state with the excitation energy  $\varepsilon$  and  $\mathcal{F}_m(\varepsilon, t_1, t_2)$  is the probability that the excited  $C_{60}^{+*}$  ion with the energy  $\varepsilon$  (plus the internal energy of the neutral  $C_{60}$ ) will decay in the time window  $(t_1, t_2)$  into fragment ion  $C_{60-2m}^+$ . The function  $\mathcal{F}_m(\varepsilon, t_1, t_2)$  is simply the breakdown curve for the fragmentation process  $C_{60}^+ \rightarrow C_{60-2m}^+$ , convoluted with the internal energy distribution of the neutral  $C_{60}$ . It follows from (6) that the breakdown curve  $\mathcal{F}_m(\varepsilon, t_1, t_2)$  is proportional to the second derivative of the ionization cross-section curve for the fragment ion  $C_{60-2m}^+$ . In figure 12(a) we have plotted these second derivatives for fragment ions  $C_{58}^+$  through  $C_{48}^+$ . Note that these experimentally-derived curves differ from the (normalized) theoretical breakdown curves by the factor  $Kf(\varepsilon)$ . Since the function  $f(\varepsilon)$  varies with energy  $\varepsilon$  much slower than the breakdown curve  $\mathcal{F}_m(\varepsilon, t_1, t_2)$  ([19]), the abundance maxima in both the theoretical and the experimental breakdown graphs will be located at the same energies. In a next step, we calculate the theoretical breakdown graph of  $C_{60}$  by solving a set of kinetic equations for consecutive  $C_2$  loss from the  $C_{60}^{+*}$  ion. The fragmentation rate for each sequential fragmentation step has been calculated using the RRKM formula [107]

$$k(\varepsilon) = \frac{\alpha G^*(\varepsilon - E_0)}{hN(\varepsilon)}. \quad (7)$$

Details of the calculation have been reported in [19]. Figure 12(b) shows the breakdown graph calculated using the dissociation energies  $E_a$  from table 2. As can be seen, there is good agreement for the positions of the abundance maxima in the  $C_{58}^+ - C_{48}^+$  breakdown curves between the experimental and the calculated breakdown graphs. This proves that the two-step procedure used here for the first time is internally self-consistent.

The experimental and the calculated breakdown graphs differ in the magnitudes of the abundance maxima, i.e. in the experimental breakdown graph (figure 12(a)) the fractional abundance of the fragment ions  $C_{60-2m}^+$  decreases very rapidly with increasing  $m$ . We attribute this effect to the decreasing density of states and excitation cross-sections of the  $C_{60}$  molecule with increasing excitation energy  $\varepsilon$  thereby leading to decreasing energy deposition function  $Kf(\varepsilon)$ . This decrease can be offset by proper normalization of the experimental breakdown graph [34, 108]. The agreement between the experimental (figure 12(a)) and the corrected calculated (figure 12(c)) breakdown graphs is very good, both in the peak positions and in the relative peak abundances (for more details see [34]), thus confirming the reliability of the binding energies given in table 2.

## 5. Stability of singly- and multiply-charged fullerenes

### 5.1. Unimolecular decay of singly-charged fullerene ions

The dissociation energetics and dynamics of excited fullerene parent ions, e.g.  $C_{60}^{+*} \rightarrow$  fragment ions, are still a matter of controversy. On the one side as mentioned above, reported dissociation energies for the loss of a neutral  $C_2$  unit do not yet con-

verge to a common value (figure 11), whilst on the other hand the competition between different dissociation channels is a closely-related issue not yet understood completely. Collision-induced [61, 99, 109–111] or photon-induced [60, 112, 113] dissociation of  $C_{60}^+$  leads to large yields of even-sized fragment ions down to around  $C_{30}^+$ . Moreover, formation of  $C_{60}^+$  via electron impact ionization (see above) or multiphoton excitation [98] is always accompanied by an abundant series of even-sized fragment ions (with almost exponential decreasing abundance), unless in the case of multiphoton-excitation the photon energy exceeds about 5.8 eV [98, 114] or the duration of the photon pulse is about  $10^{-12}$  s or less [115]. One of the central questions arising from these studies has been whether the fragment ions produced, i.e.  $C_{58}^+$ ,  $C_{56}^+$ , ..., result from sequential loss of  $C_2$  units via reactions



or whether they are produced by fission (cleavage) reactions involving the direct loss of larger, even-sized fragments via



with  $m = 1, 2, \dots$

It is clear that the occurrence and the relative probability of these two reaction channels may depend (i) on the time window probed after the production of the initial excited  $C_{60}$  ion and (ii) on the amount and manner of deposition of energy into this parent ion, and thus on the experimental set-up used to study these dissociation reactions. Moreover, neutral or charged fragments produced in an initial multiphoton dissociation reaction may absorb additional photons if photon pulses of more than 10 ns duration are used, thereby initiating a chain of excitation/dissociation cycles.

While several recent reports [28, 111, 116] have emphasized that loss of  $C_4$  or larger even-sized clusters may be an important dissociation channel under certain circumstances, the sequential metastable loss of two or more  $C_2$  units from fullerene ions (assumed to be the dominant channel in the various RRKM calculations [19, 44, 108] on the decay of  $C_{60}^+$ ) has not yet been identified. For instance, detailed analysis (see also below) of charge separation reactions of the type  $C_{60}^{z+} \rightarrow C_{56}^{(z-1)+}$  (with  $z = 4-6$ ) have led to the conclusion that these reactions are initiated by the statistical evaporation of a  $C_4$  unit followed by a charge-transfer reaction between the emitted  $C_4$  and the remaining highly-charged fullerene ion [28]. McHale *et al.* [111], employing collision-induced dissociation of  $C_{60}^{z+}$  (with  $z$  up to 3) followed by collisional re-ionization of the neutral fragments produced, conclude that unimolecular decomposition into fragments of size  $C_{56}$  ions and less proceed by elimination of units larger than  $C_2$ . Lykke and co-workers [116] have also identified  $C_4$  among neutral fragments of multiphoton-excited  $C_{60}$ , but could not quantify its abundance. Likewise, Campbell and co-workers [60, 113] concluded that ejection of  $C_n$  with  $n > 2$  is the dominant fragmentation process for highly-excited fullerenes; they do not observe any evidence in their photoionization experiments for sequential evaporation of  $C_2$  in the metastable time regime.

On the other hand, if the discussion is restricted to metastable reactions of positively-charged fullerenes, loss of  $C_2$  is always found to be the most abundant decay reaction with (i) metastable fractions (reaction rates) comparable to the case of monomer evaporation for ionized van der Waals clusters [117] (figure 13) and with (ii) a mirror-like correspondence between the mass spectral distribution and the decay rates (figure 13) also known from ionized van der Waals clusters [118] and in line with predictions from the Klotz evaporative ensemble theory [119]. Moreover, metastable

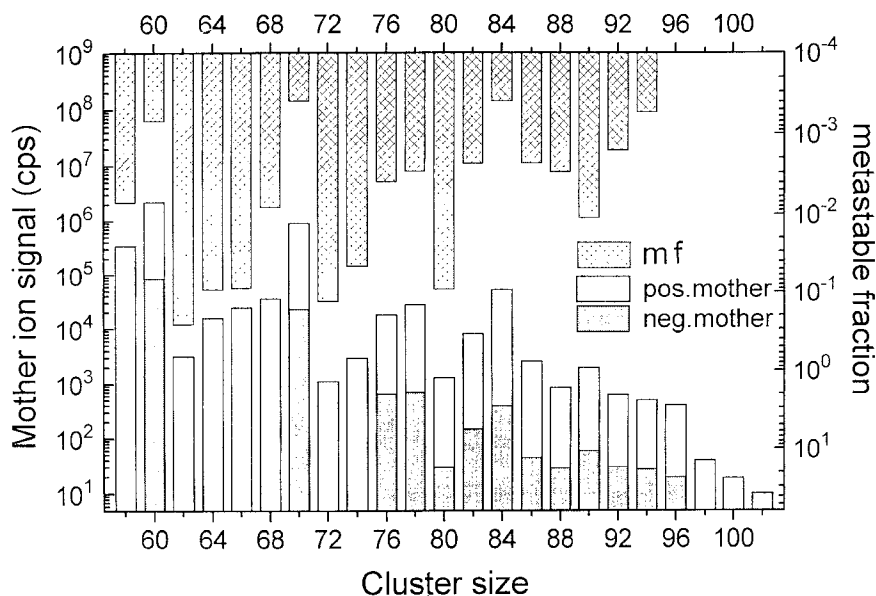


Figure 13. Mass spectrum (left hand scale) and metastable fraction,  $mf$ , (daughter ion divided by parent ion abundance, right hand scale) for carbon cluster ions (produced by electron impact ionization and electron attachment of a fullerene beam containing  $C_{60}$  and  $C_{70}$ ) as a function of cluster size.

decay of  $C_{60}^+$  into  $C_{56}^+$  has also been observed [35, 53]—though at much slower rates—but it has not been possible to identify the nature of the products, i.e.  $C_4$  or two  $C_2$  units.

As recent tight binding molecular dynamics simulations of  $C_2$  loss from  $C_{60}$  unambiguously support sequential  $C_2$  loss rather than  $C_4$  or  $C_6$  loss, since the latter always cause the cage to shatter before it can reclose all the broken bonds [103, 120], we have made a thorough analysis [35] of the metastable compositions of positively-charged fullerene ions  $C_{60}^{z+}$  and  $C_{58}^{z+}$  ions with  $z = 1-3$  using a technique where the two field-free regions of the double focussing sector field mass spectrometer are used as independent time windows [50]. As shown in figure 14 we find conclusive evidence for the occurrence of the sequential reactions (8a) for these parent ions.

### 5.2. Charge separation reactions of multiply-charged fullerene ions

Whereas knowledge about the production and the properties of highly-charged atomic ions has advanced rapidly in the past decade [121], much less attention has been directed towards polyatomic cations with more than two charges. One of the reasons for the lack of studies and data on highly-charged molecular ions is their rapidly increasing instability with charge state  $z$  due to the repulsive Coulomb forces acting between the localized charges at different sites of the molecule. Stable higher charge states are observed only for very large molecular systems, for instance for atomic or molecular clusters with sizes exceeding a critical size  $n_c(z)$  for which the Coulombic repulsion between the singly-charged cluster constituents (distributed over the cluster surface) is smaller than the bonding forces [122]. The lowest observed sizes for multiply-charged weakly-bound clusters are those for  $C_6H_6$  clusters [123] with measured appearance sizes of 52 and 92 for triply- and quadruply-charged cluster ions, respectively.



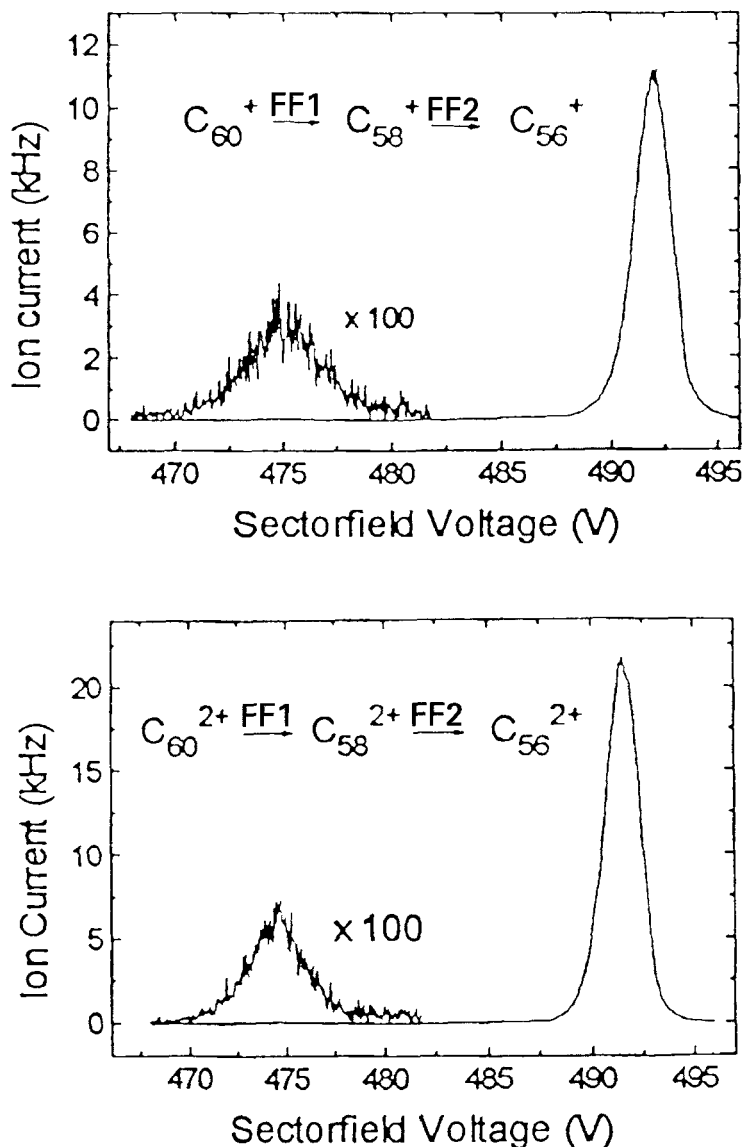


Figure 14. Metastable peaks (left hand side) corresponding to the sequential decay reactions  $C_{60}^{z+} \rightarrow C_{58}^{z+} \rightarrow C_{56}^{z+}$  in the first and second field-free region respectively, for charge states  $z = 1$  and 2. The peaks on the right hand side correspond to the simple decay reaction  $C_{60}^{z+} \rightarrow C_{58}^{z+} + C_2$  in the first field-free region.

In contrast, most of the already known doubly-charged (small) molecular ions are not stable, their existence on the metastable time regime in a mass spectrometer being due either to valence forces leading to local minima in the otherwise repulsive Coulomb states or to charge polarization states correlating for heteronuclear diatomic species  $AB$  to  $A^{2+} + B$  [124–126]. There exist only a few doubly-charged molecular ions which are thermodynamically stable, i.e. lying below the lowest dissociation limits [127, 128]. Recently, Radom and co-workers [129] have predicted from *ab initio* calculations the possible kinetic stability (inhibition of the Coulombic repulsion by

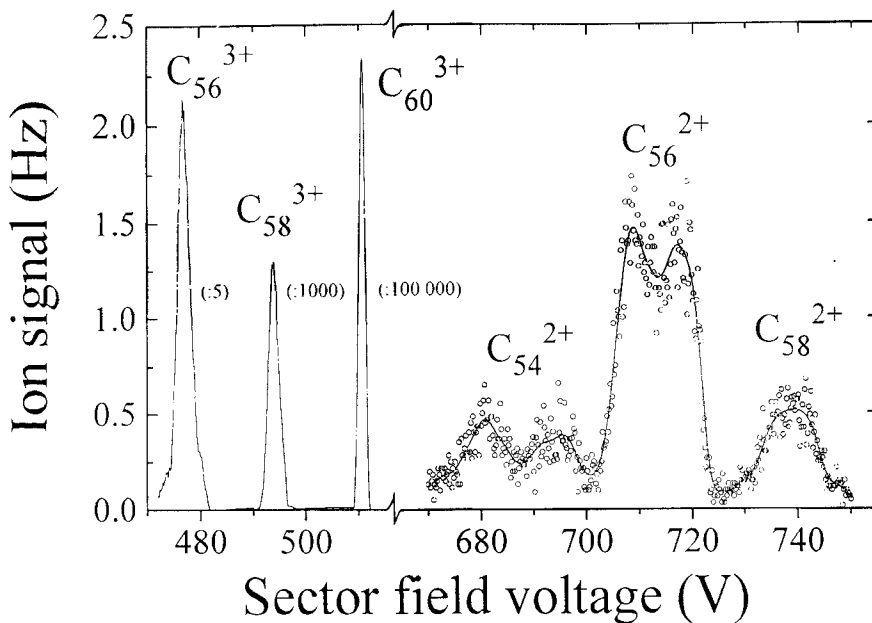


Figure 15. Parent mass peak  $C_{60}^{3+}$  and MIKE-scans of the fragment ion peaks corresponding to the decay reactions in the first field-free region  $C_{60}^{3+} \rightarrow C_{58}^{3+} + C_2$ ,  $C_{60}^{3+} \rightarrow C_{56}^{3+} + C_4$  (or  $C_2 + C_2$ ),  $C_{60}^{3+} \rightarrow C_{58}^{2+} + C_2$ ,  $C_{60}^{3+} \rightarrow C_{56}^{2+} + C_4$ , and  $C_{60}^{3+} \rightarrow C_{54}^{2+} + C_6^+$ .

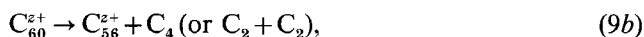
an energy barrier which is sufficiently high to permit experimental observation) of quadruply-charged molecular ions, however, so far, only triply-charged (small) molecular cations have been observed with mass spectrometers [130–132].

In the present study we have presented the production and observation of molecular ions with charge states up to 7, including  $C_{60}^{7+}$ ,  $C_{70}^{7+}$  and other buckminsterfullerene ions. Their stability can be studied by metastable mass spectrometry techniques [49, 50] allowing the identification of spontaneous decay reactions and their mechanisms. It is possible for the first time to (i) determine the corresponding energy release and (ii) study the reaction kinetics for the decay of molecular ions with charge states higher than 2. A first partial account of these results has been given in [29]. In this paper a special effort is made to discuss on the one hand the decay reactions and mechanisms for these highly-charged ions, and on the other hand to summarize evidence in favour of the proposed auto-charge transfer (ACT) reaction held responsible for the observed super-asymmetric charge separation reactions of these highly-charged molecular ions.

Besides the well-known (and up to charge state +2 well-characterized [19, 34, 35, 55, 56]) dissociation reaction involving a  $C_2$  evaporation



and a much less probable  $C_4$  evaporation (see above)



multiply-charged  $C_{60}$  ions with a charge state of 3 to 7 have been found in our recent studies (e.g. figure 15) to decay spontaneously via a super-asymmetric charge separation reaction involving the loss of a charged  $C_2^+$  fragment ion



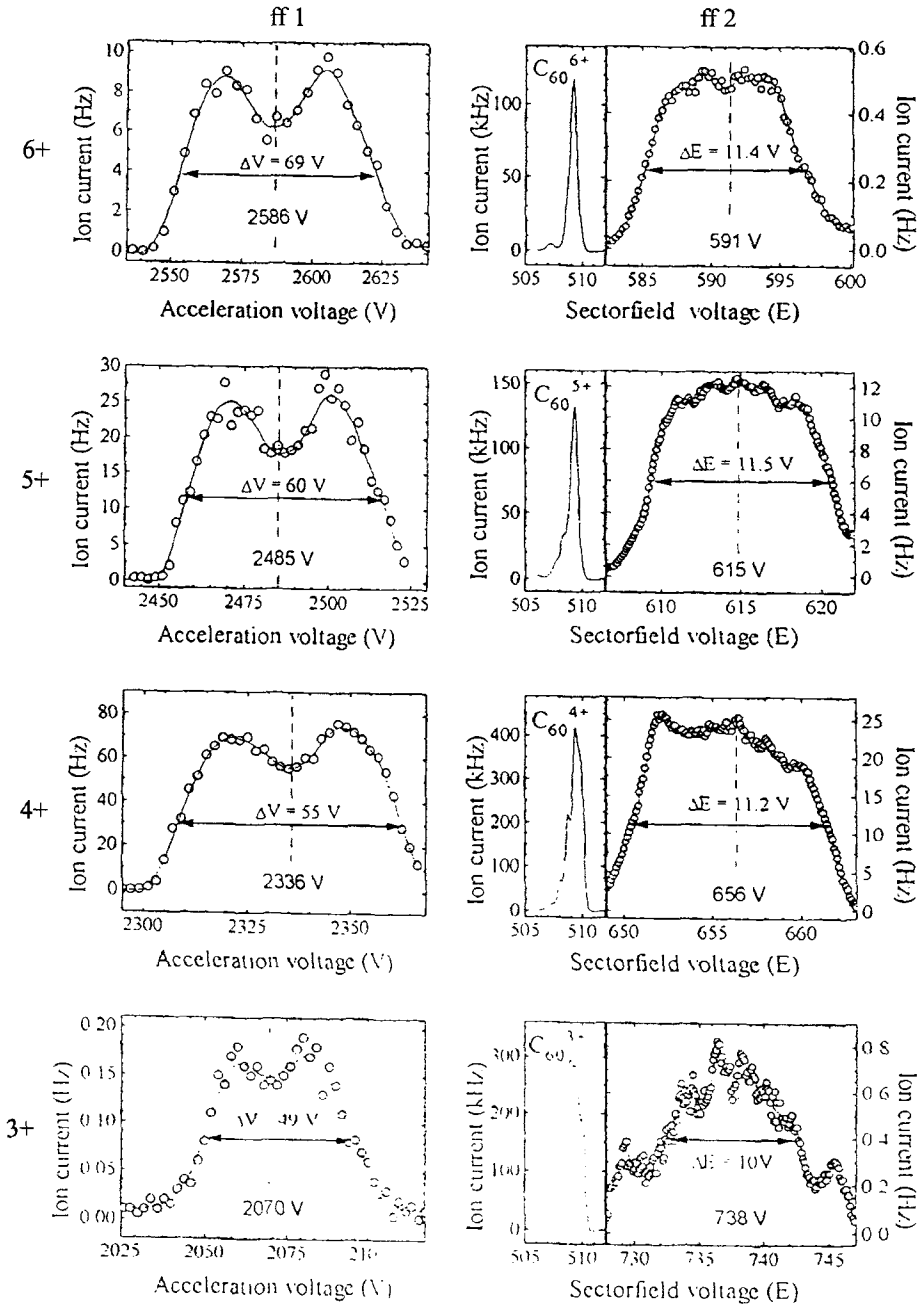


Figure 16. Metastable peaks corresponding to spontaneous decay reactions  $C_{60}^{z+} \rightarrow C_{58}^{(z-1)+} + C_2^+$  (for precursor ions with charge states 3 to 6) in the first field-free region (left hand side) and second field-free region (right hand side) as measured by the HV- and MIKE-scan technique. Also shown for comparison in the right hand case are the corresponding precursor ion peaks.

The only other spontaneous decay reactions identified in the present study by the presence of metastable peaks—though with much lower reaction probabilities—are the loss of charged  $C_4^+$  and  $C_6^+$  fragment ions ([28, 42]).

Figure 16 gives examples for measured ion kinetic energy spectra (see above) for the decay reaction (10) observed for charge states 3 to 6 (the corresponding HV-scan peak for charge state +7 has been shown in [25]). Whereas the metastable peaks on the left hand side of figure 16 are obtained by HV-scans of the metastable transitions in the first field-free region, the data on the right hand side are MIKE-scans in the second field-free region (for comparison the corresponding mass peaks of the precursor ion is also shown). The HV-scans show the broad dished peak shape which is typical [49] of metastable transitions (without interference from collision-induced dissociations) associated with (i) a rather large kinetic energy released in the course of the decay and (ii) a relatively long flight path before detection of the ions. Moreover as can be seen the minimum of the dished peaks is close to the exact position of the metastable transition (see eqn. (1)), which is designated with a dashed line in figure 16. Whereas the width of the peaks is due to the kinetic energy release during the decay in the forward and backward direction, respectively, the minimum in the peaks is caused by discrimination for those ions which are accelerated by this energy perpendicular to the flight direction. In the case of the MIKE-scans (second field-free region), discrimination is less severe due to the much shorter final flight path (the exact position of the metastable transition as given by (2) is indicated by a dashed line in figure 16).

As the precursor ion peak already has a certain width in the HV- or MIKE-scan (figure 16) the width of the daughter ion peak is only in part a result of the kinetic energy release  $E_{\text{kin}}$  during the decay. In a first approximation  $E_{\text{kin}}$  is proportional to the FWHM of the daughter ion peak, taking into account the FWHM of the precursor ion, where the latter has to be corrected by the factor  $U^*/U$  or  $E^*/E$  ( $U^*$  and  $E^*$  are the acceleration or sector field voltage at the peak centre of the daughter ion,  $U$  and  $E$  of the precursor ion, respectively) [133]. According to Beynon and co-authors [49], for simple charge separation reactions the translational energy release  $E_{\text{kin}}$  can be calculated from the corrected width of the metastable peaks  $\Delta V_c$  and  $\Delta E_c$  using

$$E_{\text{kin}} = \frac{z_1^2 m_2^2 e V}{16 z_2 m_1 m_3} \left( \frac{\Delta V_c}{V} \right)^2 \quad (11)$$

and

$$E_{\text{kin}} = \frac{z_2^2 m_1^2 e V}{16 z_1 m_2 m_3} \left( \frac{\Delta E_c}{E} \right)^2 \quad (12)$$

where  $z_1$  and  $m_1$  are the charge state and mass of the precursor ion,  $z_2$  and  $m_2$  are the charge state and mass of the detected fragment ion,  $m_3$  is the mass of the undetected fragment ion  $C_2^+$ ,  $V$  is the correct acceleration voltage and  $E$  is the correct sector field voltage for the detection of the precursor ion. Figure 17 gives the calculated  $E_{\text{kin}}$  data for decay reactions (10) as a function of the charge state  $z$  for both field-free regions. Within the experimental error bars no dependence of the  $E_{\text{kin}}$  on the time since production of the precursor ion can be seen, i.e. the energy released is the same for the two experimental time windows (first and second field-free region, respectively). In contrast, the energy released depends strongly on the charge state.

Assuming that the kinetic energy released in the metastable transition is a consequence of the Coulomb repulsion between the two fragment ions the interchange distance of the transition state can be calculated with the help of the Coulomb law. For

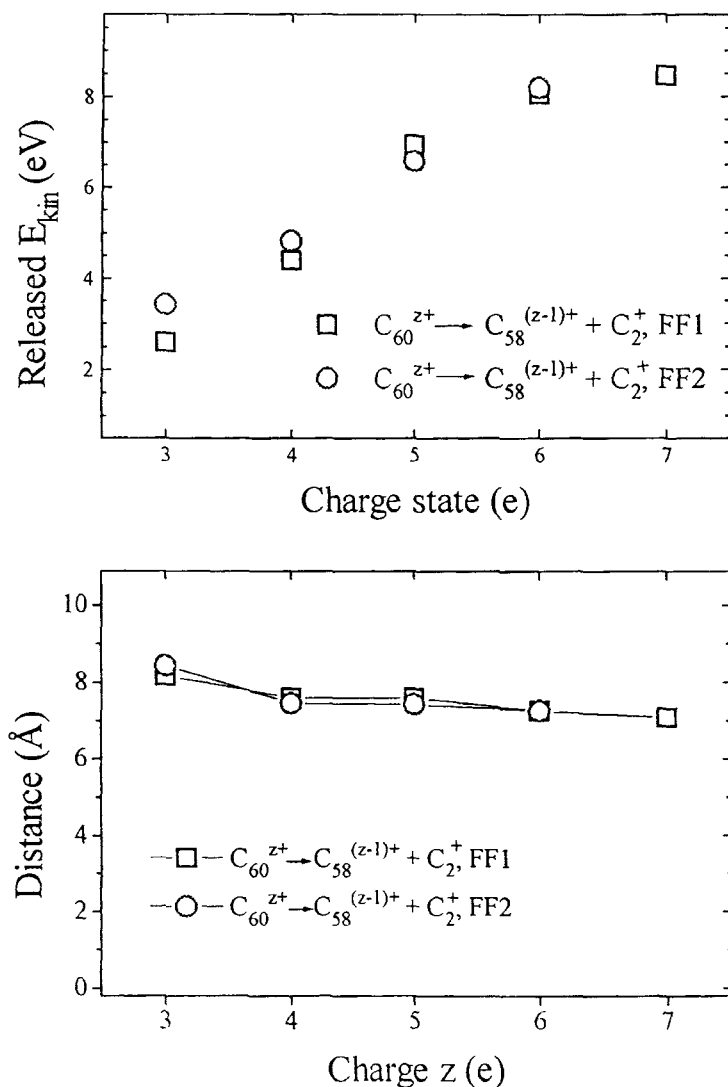


Figure 17. Kinetic energy release (upper part) and apparent intercharge distance (lower part) as a function of the precursor ion charge state in the first field-free region (FF1) and in the second field-free region (FF2).

the simple case of two singly-charged separating fragment ions and under the assumption that these fragment ions can be treated as point charges, the intercharge distance follows from

$$E_{\text{kin}} = \frac{1}{4\pi\epsilon_0} \frac{z_2(z_1 - z_2)e^2}{R}. \quad (13)$$

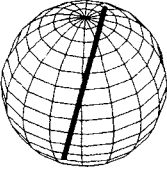
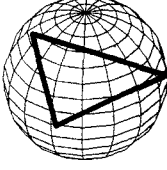
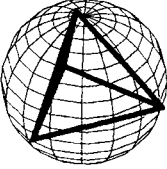

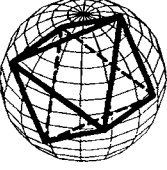

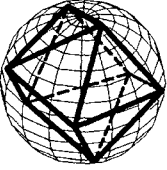
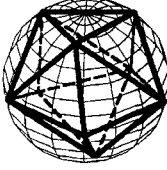
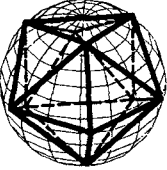
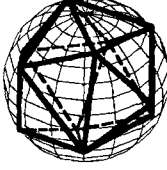
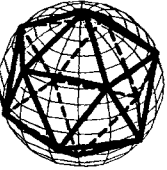
In the present case, however, one of the separating fragment ions carries more than one charge and these charges are located at different positions on a large molecule. Therefore the two separating fragment ions cannot be approximated by point charges and relaxation effects have to be taken into account.

According to Peterson and co-workers [134] the observed stability of  $C_{60}$  polycations up to  $z = 4$  indicates that charge shielding and/or delocalization inhibits

the fragmentation, because following the model of Bennemann and co-workers [135] (which proposes that the criterion for Coulombic decay of multiply-charged metallic, ionic or van der Waals-type clusters is that the Coulomb repulsion between the charged fragments exceeds the binding energy between these fragments), they estimate using a binding energy of 4.6 eV for  $C_2$  in  $C_{60}^+$  [136] that a spherically symmetric  $C_{60}^{4+}$  ion would be unstable against Coulombic decay. Bohme and co-workers [94], however, recently pointed out that the arguments of Peterson and co-workers ignore the difference in character between the chemical bonding within the fullerene frame and the electrostatic repulsion between the multiple charges. Bohme and co-workers argue that in the case of  $C_{60}^{4+}$  the chemical bonding between the two charged fragments will be essentially dissipated at a separation of the  $C_2^+$  from the surface of the remnant fullerene cage of only 2–3 Å, whereas at this separation considerable Coulomb repulsion of 5.5 eV or more remains for the  $C_2^+$  from the Coulomb repulsion of 7.55 eV for a symmetric charge distribution on the fullerene cage surface. The Coulomb energy thus released over this separation, to counteract the chemical bonding, is only approximately 2.0 eV, which is not sufficient to permit this fragmentation. Similar arguments have been advanced by Bohme and co-workers for the likely stability of  $C_{60}^{5+}$  and  $C_{60}^{6+}$  against Coulomb repulsion. In order to explain the present results, however, it is necessary to extend these arguments of Bohme and co-workers in such a way that it is possible to account for the existence of up to septuply-charged fullerene ions. They used as a basis for the Coulomb energy release a total Coulomb energy calculated for a  $C_{60}$  polycation of radius equal to that of the parent neutral cage (3.5 Å [137]), upon which all charges are at any point in time at the maximum mutual separation attainable upon a sphere of this size. This optimization procedure [31] gives, at least for charges up to 8, simple geometric configurations as shown in table 3. For instance, the most stable  $C_{60}^{7+}$  charge distribution consists of a pentagonal bipyramid, leading to a total Coulomb energy of 59.42 eV and amounting to an increase in  $V_{tot}$  from  $C_{60}^{6+}$  to  $C_{60}^{7+}$  of 18.34 eV. As the Coulomb repulsion between a pentagonal charge and the other six is with 17.14 eV larger than the repulsion of 16.60 eV for a charge located at the pole position, the energetically most favourable dissociation path is the ejection of the pentagonal charge. Following Bohme and co-workers, however, at a distance of 3 Å, where the chemical bonding will be dissipated, at least 11.98 eV remains from the original Coulomb repulsion. Thus the Coulomb energy released over this distance is about 5.1 eV, which is still smaller than the generally accepted value for the binding energy of  $C_2$  to  $C_{58}$  which is in the order of 7 eV [19]. This energy release is therefore not sufficient to promote immediate Coulomb explosion unless the bonding energy is much weaker than in the neutral or singly-charged  $C_{60}$ . According to these considerations we predict the existence of highly-charged fullerene ions with charges up to around at least 8 or 9 (the recent observation of octuply-charged fullerene ions is described in [31, 33, 36, 39]). Moreover, it is clear that if one charge is removed from its surface position (i.e. a  $C_2^+$  ion is emitted) to a certain distance away from the surface, the remaining charges will relax to different positions on the surface accordingly. Only in the limit of large distances will the fullerene fragment ion change from the charge configuration of the precursor ion to the ground state distribution of a fullerene ion having one charge less (for instance by such a charge separation reaction the pentagonal bipyramidal  $C_{60}^{7+}$  will eventually end up in an octahedral  $C_{58}^{6+}$  of slightly smaller size).

Therefore taking into account screening effects and the relaxation of the charges on the fullerene cage as the reaction products separate (for more details see [29, 31, 33]),

Table 3. Total Coulombic repulsion  $V_{\text{tot}}$  and schematic charge configuration existing between the charges on the polycations  $C_{60}^{z+}$  ( $z = 2-12$ ).

$z = 2$ , linear $V_{\text{tot}} = 2.06 \text{ eV}$		$z = 3$ , triangle $V_{\text{tot}} = 7.13 \text{ eV}$	
pairs of charges: 1 edges: 1 faces: 0		pairs of charges: 3 edges: 3 faces: 1	
$z = 4$ , tetrahedron $V_{\text{tot}} = 15.1 \text{ eV}$		$z = 5$ , trigonal bipyramid $V_{\text{tot}} = 26.64 \text{ eV}$	
pairs of charges: 6 edges: 6 faces: 4		pairs of charges: 10 edges: 9 faces: 6	
$z = 6$ , octahedron $V_{\text{tot}} = 41.08 \text{ eV}$		$z = 7$ , pentagonal bipyramid $V_{\text{tot}} = 59.42 \text{ eV}$	
pairs of charges: 15 edges: 12 faces: 8		pairs of charges: 21 edges: 15 faces: 10	
$z = 2$ , twisted cube $V_{\text{tot}} = 80.89 \text{ eV}$		$z = 9$ $V_{\text{tot}} = 105.91 \text{ eV}$	
pairs of charges: 28 edges: 16 faces: 10		pairs of charges: 36 edges: 21 faces: 14	
$z = 10$ , like $z = 8$ with 2 poles $V_{\text{tot}} = 134.51 \text{ eV}$		$z = 11$ $V_{\text{tot}} = 166.91 \text{ eV}$	
pairs of charges: 45 edges: 24 faces: 16		pairs of charges: 55 edges: 27 faces: 18	
$z = 12$ , icosahedron $V_{\text{tot}} = 202.14 \text{ eV}$			
pairs of charges: 66 edges: 30 faces: 20			

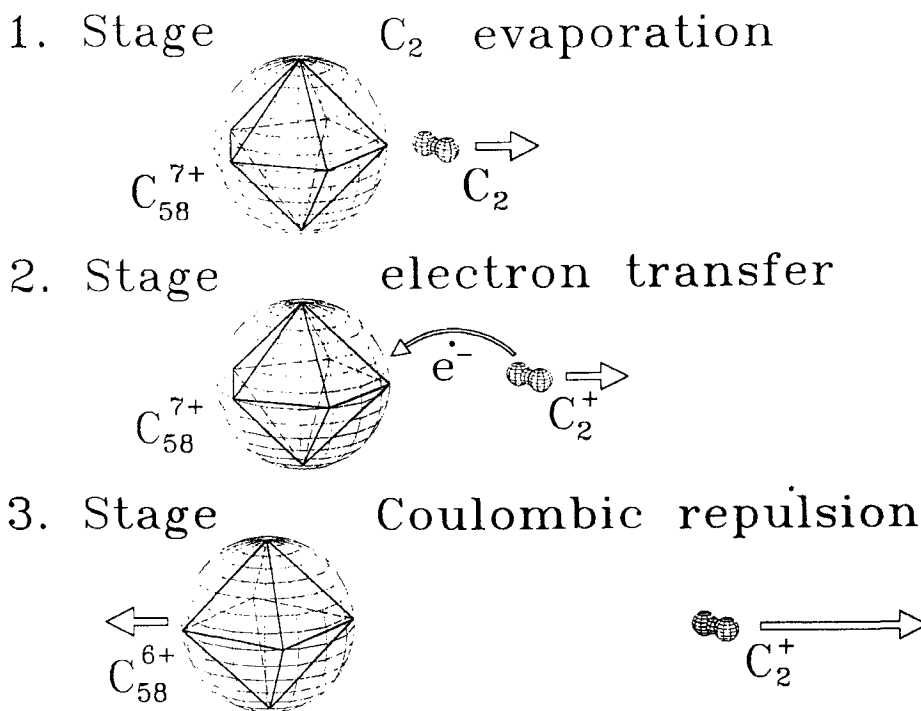


Figure 18. Schematic view of the three-stage reaction sequence responsible for the super-asymmetric charge separation reaction  $C_{60}^{z+} \rightarrow C_{58}^{(z-1)+} + C_2^+$ .

we have calculated from the experimental  $E_{\text{kin}}$  data the corresponding interchange distance of the transition states as a function of the precursor charge state  $z$ . The results obtained are shown in the lower part of figure 17. The data for the interchange distance decrease slightly with increasing charge state from a value of approximately 8 Å to 7 Å. Quite surprisingly these apparent interchange distances derived from the experimental data are approximately a factor of two larger than (i) the radius of the parent neutral,  $r(C_{60}) = 3.5$  Å [137]), (ii) the radius of any of the higher-charged  $C_{60}$  polycations [138, 139] and (iii) the radius of highly excited fullerenes (as has been shown in recent *ab initio* and molecular dynamics calculations [103, 140]).

Based on this rather characteristic experimental finding (i.e. the significant discrepancy between the radius of  $C_{60}$  and the apparent interchange distance of the separating fragment ions), we recently proposed the following three-stage decay mechanism to be responsible for the observed super-asymmetric fission reactions (10) of the highly-charged  $C_{60}^{z+}$  ions: *Reaction (10) proceeds via three different stages (visualized schematically in figure 18 for the case of  $C_{60}^{7+}$ ). This reaction sequence is initiated by the statistically-driven evaporation of a neutral  $C_2$  unit (reaction (9a)). It is followed in the second stage by an electron transfer process between the receding  $C_2$  fragment and the remaining highly-charged fullerene cage. This charge transfer occurs at the above-determined interchange distance of about 7–8 Å. In the final stage the Coulomb repulsion between the two nascent charged fragments imparts to the fragments the kinetic energy responsible for the width of the metastable peaks.*

In the following we will discuss further experimental facts and theoretical arguments in support of this novel auto-charge transfer (ACT) reaction sequence. Clearly the initial clue came from the observed large apparent interchange distance,



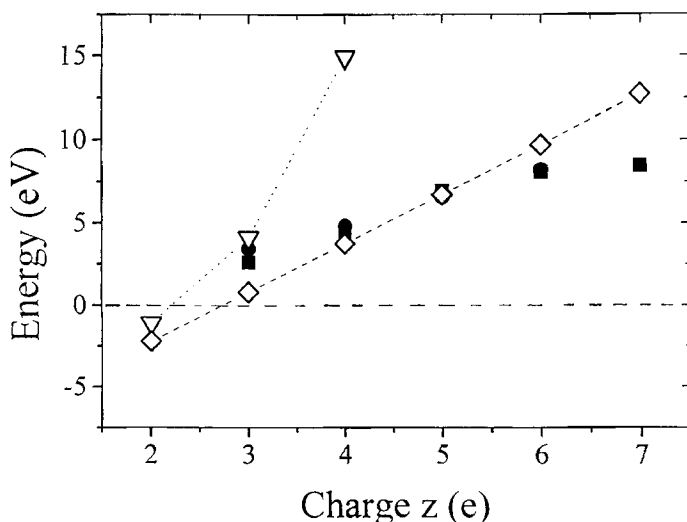


Figure 19. Kinetic energy release versus precursor ion charge  $z$  in the first field-free region (filled squares), and in the second field-free region (filled circles) as shown in figure 17. According to [32] this experimental energy release can be (due to energy conservation) at the most equal to the difference in the ionization energies  $IE$  before and after the decay reaction, i.e.  $IE(C_{60}^{z+}) - IE(C_{58}^{(z-1)+}) - IE(C_2)$ . Calculated differences using the experimental ionization energies and theoretical predictions by Yannouleas and Landman [74], respectively, are plotted as open triangles and open diamonds. Note that for  $z = 2$  both calculations yield negative values thus indicating that the decay reaction is endothermic.

which cannot be reconciled with the properties expected in the case of a single-step fissioning reaction (where the eventually charged fission products may be already distinguishable at a rather early stage of the fission process) known from nuclear physics and described in the frame of the Liquid Drop Model (LDM) [141]. Despite its successful application in the case of multiply-charged cluster ions [122, 142, 143] the LDM would predict much smaller intercharge distances than the ones derived here.

A rather striking argument in favour of the present interpretation is the complete absence of the charge separation reaction (10) for doubly-charged fullerene ions. In the case of a single-step fissioning reaction there is no reason for this conspicuous absence, whereas if reaction (10) proceeds via the three-stage sequence outlined above the electron charge transfer (second stage) is endothermic for precursor ions with less than three charges (see figure 19 showing the calculated energy balance) and thus cannot proceed (for more details see [29, 32] and references given therein).

Another important confirmation for the concept of the ACT reaction sequence can be obtained from the time-dependence of the reaction rate constants of the decay reactions. For all charge states higher than 2 and lower than 7 both the neutral and charged  $C_2$  evaporation could be observed. The neutral  $C_2$  evaporation is a typical statistically-driven decay which can be described by RRKM theory or a similar statistical model. Therefore the decay rate is determined by the internal energy, the number of internal degrees of freedom and the binding energy [19, 55, 56]. Moreover, the time-dependence of the decay of an ion ensemble formed by electron impact ionization exhibits a non-exponential behaviour due to the presence of ions with a range of internal energies (see also the considerations by Klots [119] and experimental results [144]). This time-dependence can be determined in the present experiment by measuring the metastable fraction,  $mf$ , (i.e. the daughter ion signal divided by the

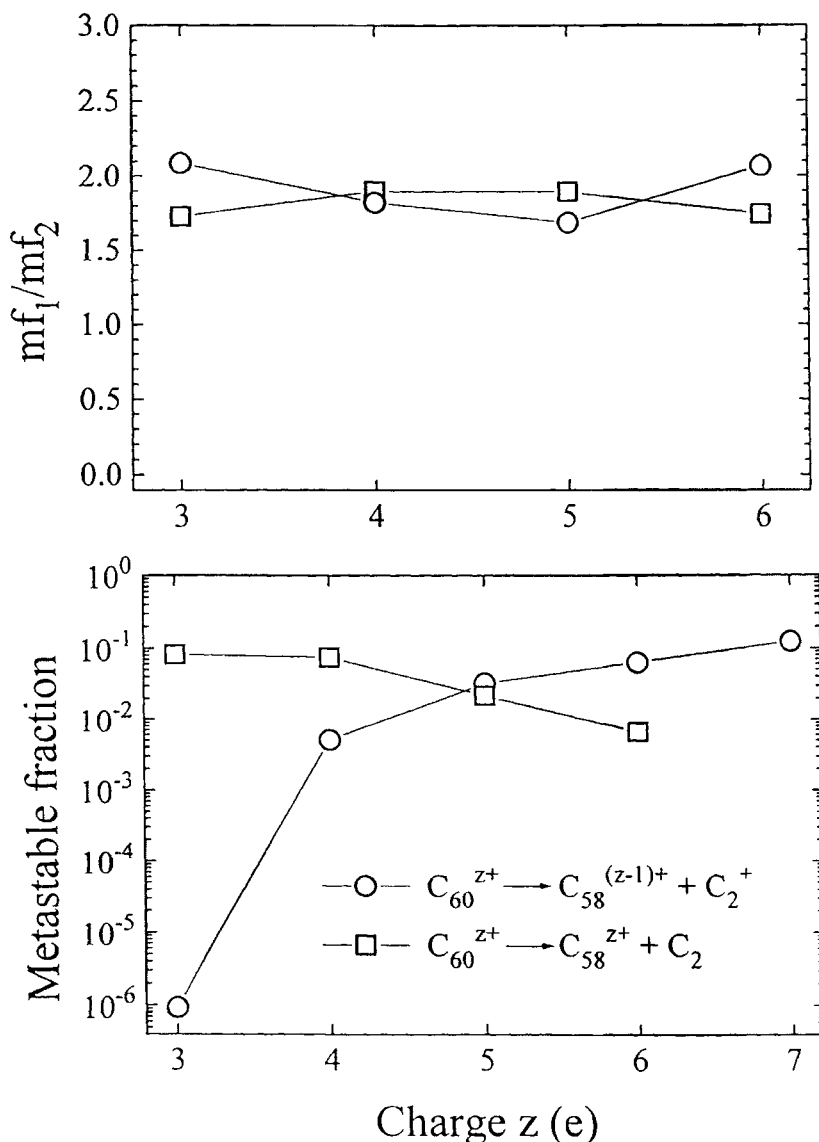


Figure 20. Upper part: Ratio of the metastable fraction (daughter ion abundance divided by the precursor ion abundance),  $mf$ , in the first field-free region and second field-free region. Lower part: Metastable fraction in the first field-free region versus precursor ion charge state for the decay involving neutral  $C_2$  evaporation (squares) and for the decay involving charged  $C_2^+$  evaporation (circles).

respective precursor ion signal) in the first and second field-free region, respectively. In order to compare the time-dependence of the  $C_2$  evaporation reaction (9a) and the charge separation reaction (10) we show in figure 20 the ratio between the metastable fraction in the first and second field-free region,  $mf_1/mf_2$ , versus the charge state for both reactions considered. In accordance with the proposed ACT reaction sequence both sets of data are independent of the charge state and match each other within the experimental error bars. This is very strong experimental evidence in favour of the three-stage mechanism, because it points out that both reactions follow the same

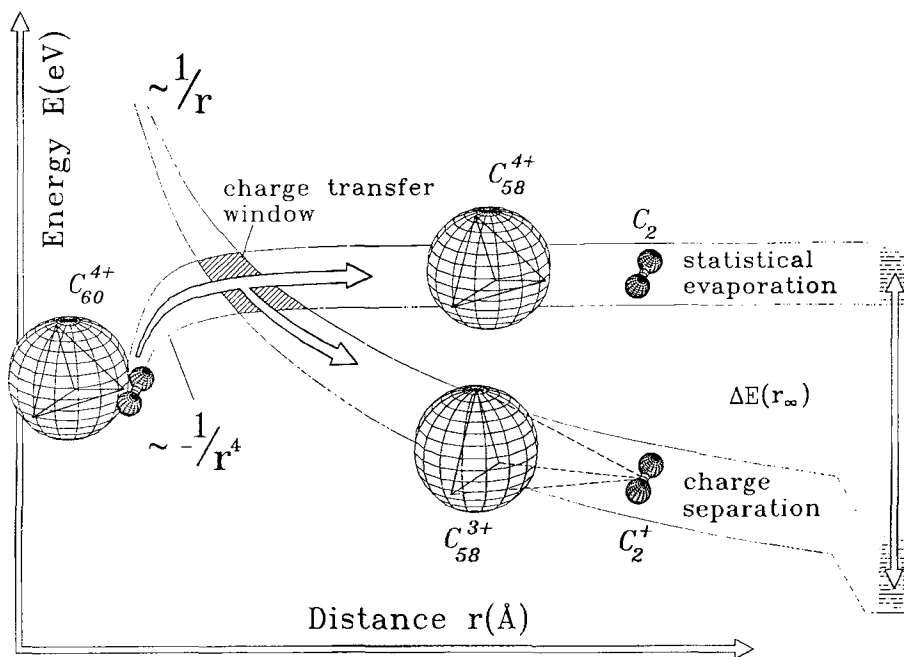


Figure 21. Schematic representation of the spontaneous decay of  $C_{60}^{4+}$  involving the (avoided) crossing of two potential curves  $C_{58}^{4+}-C_2$  and  $C_{58}^{3+}-C_2^+$ , respectively, at the internuclear distance of about 7 Å in accordance with the measured energy release  $\Delta E$  of about 4 eV.

reaction kinetics. Moreover, as can also be seen in the lower part of figure 20 (where the metastable fraction measured in the first field-free region is plotted versus charge state), the relative reaction probability for the neutral  $C_2$  evaporation and for the charge separation reaction is strongly dependent on the charge state. For low charge states the neutral evaporation is the dominant reaction path, at charge state 4 the two reactions have about equal probability and at higher charge states destruction of the highly-charged ions proceeds preferentially via the charge separation reaction. This again is in line with the present three-stage model, where it is expected that the probability of the electron transfer (i.e. the second reaction step) increases drastically with the number of charge states on the precursor ion, thereby shifting the branching ratio between the two reactions in favour of the charge separation reaction with increasing charge state.

Further supporting evidence comes from the fact that similar reactions have been observed for smaller fullerene ions [31, 33] and that the experimental results obtained for the loss of  $C_4^+$  units [28] is consistent with the ACT reaction sequence proposed. Recent studies of highly-charged  $C_{70}$  ions lend additional credence to our present interpretation [42].

Moreover, using both field-free regions as independent time windows it was possible to observe sequential  $C_2^+$  and  $C_2$  evaporations where the first decay proceeds in the first field-free region and a second evaporation from the daughter ion formed appears to happen in the second field-free region. Such a sequential evaporation sequence is very likely to occur in the aftermath of the three-stage decay mechanism proposed, because electron transfer to the highly-charged fullerene cage will lead to the release of a large amount of recombination energy in this ion and thus promote further dissociation reactions.

Charge transfer reactions between an incoming doubly-charged ion and a neutral reactant are described in ion chemistry in terms of curve crossing models, where the charge transfer occurs at the (avoided) crossing of the attractive  $r^{-4}$  ion induced dipole interaction curve (representing the incoming channel) and the repulsive  $r^{-1}$  Coulomb potential curve (representing the outgoing reaction channel). The present reaction sequence can be interpreted by this model reversing the order of the incoming and outgoing channel. This charge transfer can only take place at the crossing of the respective curves and thus will occur within a rather small reaction window (defined by the possible different states in both channels, see also [145] for more information on the existence of a reaction window) and therefore the energy released in the subsequent Coulomb repulsion will be quite well-defined. This is in accordance with the experimental results, i.e. the shape of the metastable peaks (see above). Thus the present auto-charge transfer reaction can be viewed as a charge transfer half reaction starting at the turning point of the incoming reaction channel of the well-known class of charge transfer reactions (figure 21).

### Acknowledgments

This work was partially supported by the Österreichischer Fonds zur Förderung der Wissenschaftlichen Forschung, Wien and the Bundesministerium für Wissenschaft und Forschung, Wien, Austria. Moreover, we would like to thank Prof. Dr. A. Ding (Berlin), Prof. Dr. O. Echt (Durham), Prof. Dr. C. Lifshitz (Jerusalem), Prof. Dr. C. E. Klots (Oak Ridge), and Prof. Dr. H. Schwarz (Berlin), for stimulating discussions in the course of this work.

### References

- [1] KROTO, H. W., HEATH, J. R., O'BRIEN, S. C., CURL, R. F., and SMALLEY, R. E., 1985, *Nature*, **318**, 162.
- [2] KRÄTSCHMER, W., LAMB, L. D., FOSTIROPOULOS, K., and HUFFMAN, D. R., 1990, *Nature*, **347**, 354.
- [3] KROTO, H. W., FISCHER, J. E., and COX, D. E., editors, 1993, *The Fullerenes* (Oxford: Pergamon).
- [4] LEZIUS, M., SCHEIER, P., and MÄRK, T. D., 1993, *Chem. Phys. Lett.*, **203**, 232.
- [5] ILLENBERGER, E., and MOMIGNY, J., 1992, *Gaseous Molecular Ions* (Darmstadt: Steinkopff).
- [6] HUANG, J., CARMAN, H. S., and COMPTON, R. N., 1995, *J. phys. Chem.*, **99**, 1719.
- [7] SMITH, D., SPANEL, P., and MÄRK, T. D., 1993, *Chem. Phys. Lett.*, **213**, 202.
- [8] TOSATTI, E., and MANINI, N., 1994, *Chem. Phys. Lett.*, **223**, 61.
- [9] JAFFKE, T., ILLENBERGER, E., LEZIUS, M., MATEJCIK, S., SMITH, D., and MÄRK, T. D., 1994, *Chem. Phys. Lett.*, **226**, 213.
- [10] YERETZIAN, C., HANSEN, K., and WHETTEN, R. L., 1993, *Science*, **260**, 652.
- [11] WANG, L. S., CONCEICAO, J., JIN, C., and SMALLEY, R. E., 1991, *Chem. Phys. Lett.*, **182**, 5.
- [12] MATEJCIK, S., MÄRK, T. D., SPANEL, P., SMITH, D., JAFFKE, T., and ILLENBERGER, E., 1995, *J. chem. Phys.*, **102**, 2516.
- [13] GUNNARSSON, O., HANDSCHUH, H., BECHTHOLD, P. S., KESSLER, B., GANTEFÖR, G., and EBERHARDT, W., 1995, *Phys. Rev. Lett.*, **74**, 1875.
- [14] BRINK, C., ANDERSON, L. H., HVELPLUND, P., MATHUR, D., and VOLSTAD, J. D., 1995, *Chem. Phys. Lett.*, **233**, 52.
- [15] SPANEL, P., and SMITH, D., 1994, *Chem. Phys. Lett.*, **229**, 262.
- [16] SCHAUER, S., WILLIAMS, P., and COMPTON, R. N., 1990, *Phys. Rev. Lett.*, **65**, 625.
- [17] HETTICH, R. L., COMPTON, R. N., and RITCHIE, R. H., 1991, *Phys. Rev. Lett.*, **67**, 1242.
- [18] MÄRK, T. D., and DUNN, G. H., editors, 1985, *Electron Impact Ionization* (Wien: Springer).
- [19] FOLTIN, M., LEZIUS, M., SCHEIER, P., and MÄRK, T. D., 1993, *J. chem. Phys.*, **98**, 9624.
- [20] SCHEIER, P., LEZIUS, M., DÜNSER, B., ROBL, R., SCHIESTL, B., and MÄRK, T. D., 1993, *Int. J. Mass Spectrom. Ion Processes*, **125**, R17.

- [21] LEZIUS, M., SCHEIER, P., FOLTIN, M., DÜNSER, B., RAUTH, T., AKIMOV, V. M., KRÄTSCHMER, W., and MÄRK, T. D., 1993, *Int. J. Mass Spectrom. Ion Processes*, **129**, 49.
- [22] SCHEIER, P., ROBL, R., SCHIESTL, B., and MÄRK, T. D., 1994, *Chem. Phys. Lett.*, **220**, 141.
- [23] SCHEIER, P., and MÄRK, T. D., 1994, *Int. J. Mass Spectrom. Ion Processes*, **133**, L5.
- [24] WÖRGÖTTER, R., DÜNSER, B., SCHEIER, P., and MÄRK, T. D., 1994, *J. chem. Phys.*, **101**, 8674.
- [25] SCHEIER, P., and MÄRK, T. D., 1994, *Phys. Rev. Lett.*, **73**, 54.
- [26] SCHEIER, P., DÜNSER, B., WÖRGÖTTER, R., LEZIUS, M., ROBL, R., and MÄRK, T. D., 1994, *Int. J. Mass Spectrom. Ion Processes*, **138**, 77.
- [27] MÄRK, T. D., and SCHEIER, P., 1995, *Nucl. Instrum. Methods B*, **98**, 469.
- [28] DÜNSER, B., SCHEIER, P., and MÄRK, T. D., 1995, *Chem. Phys. Lett.*, **236**, 271.
- [29] SCHEIER, P., DÜNSER, B., and MÄRK, T. D., 1995, *Phys. Rev. Lett.*, **74**, 3368.
- [30] DÜNSER, B., LEZIUS, M., SCHEIER, P., DEUTSCH, H., and MÄRK, T. D., 1995, *Phys. Rev. Lett.*, **74**, 3364.
- [31] SCHEIER, P., DÜNSER, B., and MÄRK, T. D., 1995, *J. phys. Chem.*, **99**, 15428.
- [32] SCHEIER, P., and MÄRK, T. D., 1995, *Int. J. Mass Spectrom. Ion Processes*, **146/147**, 233.
- [33] SCHEIER, P., DÜNSER, B., KIM, Y. B., and MÄRK, T. D., 1995, *Fullerene Science and Technol.* (in press).
- [34] WÖRGÖTTER, R., DÜNSER, B., SCHEIER, P., MÄRK, T. D., FOLTIN, M., KLOTS, C. E., LASKIN, J., and LIFSHITZ, C., 1995, *J. chem. Phys.*, **104**, 1225.
- [35] ECHT, O., DÜNSER, B., MÜGG, D., MATT, S., SCHEIER, P., and MÄRK, T. D., 1995, in *Proceedings of the International Symposium on the Science and Technology of Atomically Engineered materials* (Richmond).
- [36] MATT, S., DÜNSER, B., SENN, G., SCHEIER, P., and MÄRK, T. D., 1995, *Hyperfine Interactions* (in press).
- [37] MÜGG, D., MATT, S., DÜNSER, B., WÖRGÖTTER, R., LEZIUS, M., FOLTIN, M., DEUTSCH, H., BECKER, K., LASKIN, J., LIFSHITZ, C., KLOTS, C. E., SCHEIER, P., and MÄRK, T. D., 1995, in *European Network Meeting on the Structure and Reactivity of Molecular Ions* (Berlin).
- [38] MATT, S., DÜNSER, B., LEZIUS, M., DEUTSCH, H., BECKER, K., STAMATOVIC, A., SCHEIER, P., and MÄRK, T. D., 1996, *J. chem. Phys.* (in press).
- [39] RAUTH, T., ECHT, O., SCHEIER, P., and MÄRK, T. D., 1995, *Chem. Phys. Lett.*, **247**, 515.
- [40] MATT, S., WÖRGÖTTER, R., SCHEIER, P., and MÄRK, T. D., 1996, (to be published).
- [41] DÜNSER, B., MATT, S., WÖRGÖTTER, R., LEZIUS, M., FOLTIN, M., DEUTSCH, H., BECKER, K., LASKIN, J., LIFSHITZ, C., KLOTS, C. E., SCHEIER, P., and MÄRK, T. D., 1995, ICPEAC XIX (Whistler).
- [42] SENN, G., and MÄRK, T. D., 1995, Clustersymposium 95 (Potsdam).
- [43] McELVANY, S. W., ROSS, M. M., and CALLAHAN, J. H., 1992, *Accts. chem. Res.*, **25**, 162.
- [44] LIFSHITZ, C., 1993, *Mass Spectrom. Rev.*, **12**, 261.
- [45] STEPHAN, K., HELM, H., and MÄRK, T. D., 1980, *J. chem. Phys.*, **73**, 3763.
- [46] POLL, H. U., WINKLER, C., MARGREITER, D., GRILL, V., and MÄRK, T. D., 1992, *Int. J. Mass Spectrom. Ion Processes*, **112**, 1.
- [47] GRILL, V., WALDER, G., MARGREITER, D., RAUTH, T., POLL, R. U., SCHEIER, P., and MÄRK, T. D., 1993, *Z. Phys. D*, **25**, 217.
- [48] *Proceedings of the 7th International Conference on the Physics of Highly Charged Ions*, 1994, Wien, Special Issue of *Nucl. Instrum. Methods*, NIMB, i98.
- [49] COOKS, R., BEYNON, J. H., CAPRIOLI, R. M., and LESTER, G. R., 1973, *Metastable Ions* (Amsterdam: Elsevier).
- [50] SCHEIER, P., and MÄRK, T. D., 1987, *Phys. Rev. Lett.*, **59**, 1813.
- [51] VÖLPEL, R., HOFMANN, G., STEIDL, M., STENKE, M., SCHLAPP, M., TRASSL, R., and SALZBORN, E., 1993, *Phys. Rev. Lett.*, **71**, 3439.
- [52] VAN HELDEN, G., HSU, M. T., GOTTS, N., and BOWERS, M. T., 1993, *J. phys. Chem.*, **97**, 8182.
- [53] RADI, P. P., BUNN, T. L., KEMPER, P. R., MOLCHAN, M. E., and BOWERS, M. T., 1988, *J. chem. Phys.*, **88**, 2809.
- [54] RADI, P. P., HSU, M. T., BRODBELT-LUSTIG, J., RINCON, M., and BOWERS, M. T., 1990, *J. chem. Phys.*, **92**, 4817.
- [55] RADI, P. P., HSU, M. T., RINCON, M., KEMPER, P. R., and BOWERS, M. T., 1990, *Chem. Phys. Lett.*, **174**, 223.

- [56] LIFSHITZ, C., IRAQI, M., PERES, T., and FISCHER, J. E., 1991, *Int. J. Mass Spectrom. Ion Processes*, **107**, 56.
- [57] YU, D. H., ANDERSON, L. H., BRINK, C., and HVELPLUND, P., 1994, *Z. Phys. D*, **29**, 53.
- [58] CAMPBELL, E. E. B., HOHMANN, H., FURRER, S., CALLEGARI, C., KITTELMANN, O., and RINGLING, J., 1994, *Contrib. SASP 94*, edited by T. D. Mark, R. Schrittwieser and D. Smith (Maria Alm), p. 37.
- [59] GABER, H., HISS, R., BUSMANN, H. G., and HERTEL, H., 1992, *Z. Phys. D*, **24**, 302.
- [60] HOHMANN, H., EHLICH, R., FURRER, S., KITTELMANN, O., RINGLING, J., and CAMPBELL, E. E. B., 1995, *Z. Phys. D*, **23**, 143.
- [61] LEBRUN, T., BERRY, H. G., CHENG, S., DUNFORD, R. W., ESBENSEN, H., GEMMELL, D. S., and KANTER, E. P., 1994, *Phys. Rev. Lett.*, **72**, 3965.
- [62] OUASKIT, S., FARIZON, B., FARIZON, M., GAILLARD, M. J., CHEVARIER, A., CHEVARIER, N., GERLIC, E., and STERN, M., 1994, *Int. J. Mass Spectrom. Ion Processes*, **139**, 141; FARIZON, B., FARIZON, M., GAILLARD, M. J., GERLIC, E., and OUASKIT, S., *ibid.*, **144**, 79.
- [63] CAMPI, X., 1989, *Nucl. Phys. A*, **495**, 259c.
- [64] BAUER, W., 1988, *Phys. Rev. C*, **38**, 1927.
- [65] BABA, M. S., NARASIMHAN, T. S. L., BALASUBRAMANIAN, R., and MATHEWS, C. K., 1992, *Int. J. Mass Spectrom. Ion Processes*, **114**, R1.
- [66] This cross-section value has been used by our group to calibrate relative cross-section measurements for the production of  $C_{60}^+$  through  $C_{54}^+$  [20, 21]. In light of the results and discussion presented in [30, 38] this value appears to be too large.
- [67] LEZIUS, M., RAUTH, T., GRILL, V., FOLTIN, M., and MÄRK, T. D., 1992, *Z. Phys. D*, **24**, 289.
- [68] RAPP, D., and ENGLANDER-GOLDEN, P., 1965, *J. chem. Phys.* **43**, 1464; MÄRK, T. D., 1975, *ibid.*, **63**, 3731; BRINKMAN, R. T., and TRAJMAR, S., 1981, *J. Phys. E*, **14**, 245.
- [69] STANSKI, T., and ADAMCZYK, B., 1972, *Int. J. Mass Spectrom. Ion Processes*, **10**, 171; MARGREITER, D., WALDER, G., DEUTSCH, H., POLL, H. U., WINKLER, C., STEPHAN, K., and MÄRK, T. D., 1990, *ibid.*, **100**, 143.
- [70] KLINE, L. E., DAVIES, D. K., CHEN, C. L., and CHANTRY, P. J., 1979, *J. appl. Phys.*, **50**, 6789.
- [71] LIFSHITZ, C., PERES, T., KABABIA, S., and AGRANAT, I., 1988, *Int. J. Mass Spectrom. Ion Processes*, **82**, 193.
- [72] SMITH, D., 1992, *Chem. Rev.*, **92**, 1473; BOHME, D. K., 1992, *ibid.*, **92**, 1487.
- [73] PACHUTA, S. J., KANTTÄMAA, H. I., SACK, T. M., CERNY, R. L., TOMER, K. B., GROSS, M. L., PACHUTA, R. R., and COOKS, R. G., 1988, *J. Am. chem. Soc.*, **110**, 657.
- [74] YANNOULEAS, C., and LANDMAN, U., 1994, *Chem. Phys. Lett.*, **217**, 175.
- [75] STEPHAN, K., and MÄRK, T. D., 1981, *J. chem. Phys.*, **81**, 3116.
- [76] SCHEIER, P., and MÄRK, T. D., 1987, *Chem. Phys. Lett.*, **136**, 423.
- [77] BRECHIGNAC, C., BROYER, M., CAHUZAC, P., DELACRETAZ, G., LABASTIE, P., and WÖSTE, L., 1985, *Chem. Phys. Lett.*, **118**, 174.
- [78] DEUTSCH, H., BECKER, K., and MÄRK, T. D., 1995, *Int. J. Mass Spectrom. Ion Processes*, **151**, 207.
- [79] FITCH, W. L., and SAUTER, A. D., 1983, *Anal. Chem.*, **55**, 832.
- [80] MÄRK, T. D., 1984, *Electron-Molecule Interactions and their Applications*, Vol. 1, edited by L. G. Christophorou (Orlando: Academic Press), Chap. 3, p. 251.
- [81] ROSENSTOCK, H. M., DRAXL, K., STEINER, B. W., and HERRON, J. T., 1977, *J. Phys. Chem. Ref. Data*, Vol. 6, Suppl. 1.
- [82] LICHTENBERGER, D. L., JATCKO, M. E., NEBESNY, K. W., RAY, C. D., HUFFMAN, D. R., and LAMB, L. D., 1992, *Chem. Phys. Lett.*, **198**, 454.
- [83] STEGER, H., DE VRIES, J., KAMKE, B., KAMKE, W., and DREWELLO, T., 1992, *Chem. Phys. Lett.*, **194**, 452.
- [84] LIFSHITZ, C., IRAQI, M., PERES, T., and FISCHER, J. E., 1991, *Rapid Commun. Mass Spectrom.*, **5**, 238.
- [85] JAVAHERY, G., WINCEL, H., PETRIE, S., and BOHME, D. K., 1993, *Chem. Phys. Lett.*, **204**, 467.
- [86] CHRISTIAN, J. F., WAN, Z., and ANDERSON, S. L., 1993, *J. chem. Phys.*, **99**, 3468.
- [87] MATT, S., MUIGG, D., DING, A., LIFSHITZ, C., SCHEIER, P., and MÄRK, T. D., 1995, *J. phys. Chem.* (in press).

- [88] MÄRK, T. D., 1985, *Electron Impact Ionization*, edited by T. D., Märk and G. H. Dunn (Wien: Springer) Chap. 5, p. 137.
- [89] WANNIER, G. H., 1953, *Phys. Rev.*, **90**, 817; 1956, *ibid.*, **100**, 1180; DORMAN, F. H., and MORRISON, J. D., 1961, *J. chem. Phys.*, **34**, 1407.
- [90] SMITH, F. T., 1961, *J. chem. Phys.*, **34**, 793.
- [91] DE VRIES, J., STEGER, H., KAMKE, B., MENZEL, C., WEISSER, B., KAMKE, K., and HERTEL, I. V., 1992, *Chem. Phys. Lett.*, **188**, 159.
- [92] YOO, R. K., RUSCIC, B., and BERKOWITZ, J., 1992, *J. chem. Phys.*, **96**, 911.
- [93] CALDWELL, K. A., GIBLIN, D. E., and GROSS, M. L., 1992, *J. Am. chem. Soc.*, **114**, 3743.
- [94] PETRIE, S., WANG, J., and BOHME, D. K., 1993, *Chem. Phys. Lett.*, **204**, 473.
- [95] KLOTS, C. E., 1991, *Z. Phys. D*, **21**, 335.
- [96] BECK, R. D., JOHN, P. S., ALVAREZ, M. M., DIEDERICH, F., and WHETTEN, R. L., 1991, *J. phys. Chem.*, **95**, 8402.
- [97] SANDLER, P., LIFSHITZ, C., and KLOTS, C. E., 1992, *Chem. Phys. Lett.* **200**, 445.
- [98] WURZ, P., and LYKKE, K. R., 1992, *J. phys. Chem.*, **96**, 10129.
- [99] BUSMAN, H. G., LILL, T., REIF, B., and HERTEL, I. V., 1992, *Surf. Science*, **272**, 146.
- [100] ZHANG, B. L., XU, C. H., WANG, C. Z., CHAN, C. T., and HO, K. M., 1992, *Phys. Rev. B*, **46**, 7333.
- [101] STANTON, R. E., 1992, *J. phys. Chem.*, **96**, 111.
- [102] ECKHOFF, W. C., and SCUSERIA, G. E., 1993, *Chem. Phys. Lett.*, **216**, 399.
- [103] XU, C., and SCUSERIA, G. E., 1994, *Phys. Rev. Lett.*, **72**, 669.
- [104] BABA, M. S., NARASIMHAN, T. S. L., BALASUBRAMANIAN, R., and MATHEWS, C. K., 1995, *J. phys. Chem.*, **99**, 3020.
- [105] LIFSHITZ, C., 1995, private communication.
- [106] KOLODNEY, E., BUDREVICH, A., and TSIPINYUK, B., 1995, *Phys. Rev. Lett.*, **74**, 510.
- [107] FORST, W., 1973, *Theory of Unimolecular Reactions* (New York: Academic Press).
- [108] LASKIN, J., and LIFSHITZ, C., 1994, *Int. J. Mass Spectrom. Ion Processes*, **138**, 95.
- [109] DOYLE, R. J., and ROSS, M. M., 1991, *J. phys. Chem.*, **95**, 4954.
- [110] HVELPLUND, P., ANDERSON, L. H., HAUGEN, H. K., LINDHARD, J., LORENTS, D. C., MALHOTRA, R., and RUOFF, R., 1992, *Phys. Rev. Lett.*, **69**, 1915.
- [111] MCHALE, K. J., POLC, M. J., and WESDEMIOTIS, C., 1995, *J. Mass Spectrom.*, **30**, 33.
- [112] O'BRIEN, S. C., HAETH, J. R., CURL, R. F., and SMALLEY, R. E., 1988, *J. chem. Phys.*, **88**, 220.
- [113] HOHMANN, H., CALLEGARI, C., FURRER, S., GROSENICK, D., CAMPBELL, E. E. B., and HERTEL, I. V., 1994, *Phys. Rev. Lett.*, **73**, 1919.
- [114] ZHANG, Y., and STUKE, M., *Phys. Rev. Lett.*
- [115] ZHANG, Y., SPÄTH, M., KRÄTSCHMER, W., and STUKE, M., 1992, *Z. Phys. D*, **23**, 195.
- [116] LYKKE, K. R., 1995, *Electrochemistry Symposium* (Reno).
- [117] MÄRK, T. D., and ECHT, O., 1994, *Clusters of Atoms and Molecules II*, edited by H. Haberland (Berlin: Springer), Chap. 2.6, pp. 154–182.
- [118] MÄRK, T. D., 1994, *Linking the Gaseous and Condensed Phases of Matter*, edited by L. G. Christophorou, E. Illenberger, and W. F. Schmidt, NATO ASI Series B326 (New York: Plenum), pp. 155–182.
- [119] KLOTS, C. E., 1985, *J. chem. Phys.*, **83**, 5854; 1988, *J. phys. Chem.*, **92**, 5864; 1990, *Int. J. Mass Spectrom. Ion Processes*, **100**, 457.
- [120] MURRY, R. L., STROUT, D. L., and SCUSERIA, G. E., 1994, *Int. J. Mass Spectrom. Ion Processes*, **138**, 113.
- [121] MÜLLER, A., 1991, *Comments. at. molec. Phys.*, **27**, 1.
- [122] ECHT, O., and MÄRK, T. D., 1994, *Clusters of Atoms and Molecules II*, edited by H. Haberland (Berlin: Springer), Chap. 2.7, pp. 183–220.
- [123] HAHN, M. Y., SCHRIVER, K. E., and WHETTEN, R. L., 1988, *J. chem. Phys.*, **88**, 4242.
- [124] HURLEY, A. C., 1962, *J. molec. Spectrosc.*, **9**, 18.
- [125] WETMORE, R. W., LEROY, R. J., and BOYD, R. K., 1984, *J. phys. Chem.*, **88**, 6318.
- [126] KOCH, W., MAQUIN, F., STAHL, D., and SCHWARZ, H., 1985, *Chimica*, **29**, 376.
- [127] HELM, H., STEPHAN, K., MÄRK, T. D., and HUESTIS, D. L., 1981, *J. chem. Phys.*, **74**, 3844.
- [128] KOLBUSZEWSKI, M., and WRIGHT, J. S., 1994, *Chem. Phys. Lett.*, **218**, 338.
- [129] WONG, M. W., NOBES, R. H., and RADOM, L., 1987, *Rapid Commun. Mass Spectrom.*, **1**, 3.

- [130] MÄRK, T. D., 1983, *Int. J. Mass Spectrom. Ion Processes*, **55**, 325.
- [131] MORVAY, L., and CORNIDES, I., 1984, *Int. J. Mass Spectrom. Ion Processes*, **62**, 263.
- [132] SINGH, S., BOYD, R. K., HARRIS, F. M., and BEYNON, J. H., 1986, *Int. J. Mass Spectrom. Ion Processes*, **66**, 167.
- [133] BALDWIN, M. A., DERRICK, P. J., and MORGAN, R. P., 1976, *Organ. Mass Spectrom.*, **11**, 440.
- [134] BAE, Y. K., LORENTS, D. C., and PETERSON, J. R., 1992, *Chem. Phys. Lett.*, **195**, 543.
- [135] TOMANEK, D., MUKHERJEE, S., and BENNEMANN, K. H., 1983, *Phys. Rev. B*, **28**, 665.
- [136] Note that the binding energy used in this estimate is much lower than recent data [19], thus leading to an underestimation of the binding force relative to the Coulomb repulsion.
- [137] HAWKINS, J. M., MEYER, A., LEWIS, T., LOREN, S., and HOLLANDER, J. F., 1991, *Science*, **252**, 312.
- [138] HRUSAK, J., and SCHWARZ, H., 1993, *Chem. Phys. Lett.*, **205**, 187.
- [139] YAMAGUCHI, K., HAYASHI, S., OKUMURA, M., NAKANO, M., and MORI, W., 1994, *Chem. Phys. Lett.*, **226**, 372.
- [140] JING, X., and CHELIKOWSKY, J. R., 1992, *Phys. Rev. B*, **46**, 15503.
- [141] YANNOULEAS, C., BARNETT, R. N., and LANDMAN, U., 1995, *Comments. at. molec. Phys.*, **31**, 445.
- [142] KREISLE, D., ECHT, O., KNAPP, M., RECKNAGEL, E., LEITER, K., and MÄRK, T. D., 1986, *Phys. Rev. Lett.*, **54**, 1551.
- [143] BRECHIGNAC, C., CAHUZAC, P., CARLIER, F., and DE FRUTOS, M., 1994, *Phys. Rev. Lett.*, **72**, 1636.
- [144] Ji, Y., FOLTIN, M., LIAO, C. H., and MÄRK, T. D., 1992, *J. chem. Phys.*, **96**, 3624.
- [145] SMITH, D., ADAMS, N. G., ALGE, E., VILLINGER, H., and LINDINGER, W., 1980, *J. Phys. B*, **13**, 2787.